

## *Supporting Information*

### **Dual-Directional Alkyne-Terminated Macrocycles: In Route to Non-Aggregating Molecular Platforms**

Ali Husain,<sup>\*[a]</sup> Asaithampi Ganesan,<sup>[a]</sup> Basma Ghazal,<sup>[a]</sup> Mahmut Durmus,<sup>[b]</sup> Xian-Fu Zhang,<sup>[c]</sup>  
and Saad Makhseed<sup>\*[a]</sup>

<sup>[a]</sup>*Department of Chemistry, Kuwait University, P.O. Box 5969, Safat, 13060, Kuwait.*

<sup>[b]</sup>*Gebze Technical University, Department of Chemistry, 41400 Gebze-Kocaeli, Turkey.*

<sup>[c]</sup>*MPC Technologies, Hamilton, Ontario, Canada L8S 3H4.*

*\* Corresponding authors email: ali.husain@ku.edu.kw  
saad.makhseed@ku.edu.kw*

## Table of Contents

Experimental section.....	3
<b>NMR spectra.....</b>	<b>3</b>
<b>Mass spectra.....</b>	<b>14</b>
<b>MALDI-TOF-MS.....</b>	<b>14</b>
<b>ESI-MS Spectra.....</b>	<b>16</b>
Result and discussion .....	24
<b>Photophysical characterization.....</b>	<b>24</b>
<b>Ground state electronic absorption spectra of Pc1/AzaPc1 .....</b>	<b>24</b>
<b>Aggregation studies.....</b>	<b>25</b>
<b>Fluorescence measurements.....</b>	<b>27</b>
<b>Fluorescence quantum yields and lifetimes .....</b>	<b>29</b>
<b>Singlet oxygen quantum yields .....</b>	<b>30</b>
<b>Photodegradation quantum yields .....</b>	<b>31</b>
<b>Excited triplet state .....</b>	<b>32</b>
<b>Single crystal X-ray diffraction studies of propargyl functionalized phthalocyanine analogues and their precursors.....</b>	<b>35</b>
<b>Experimental .....</b>	<b>35</b>
<b>Discussion.....</b>	<b>35</b>
References .....	49

## Experimental section

### NMR spectra

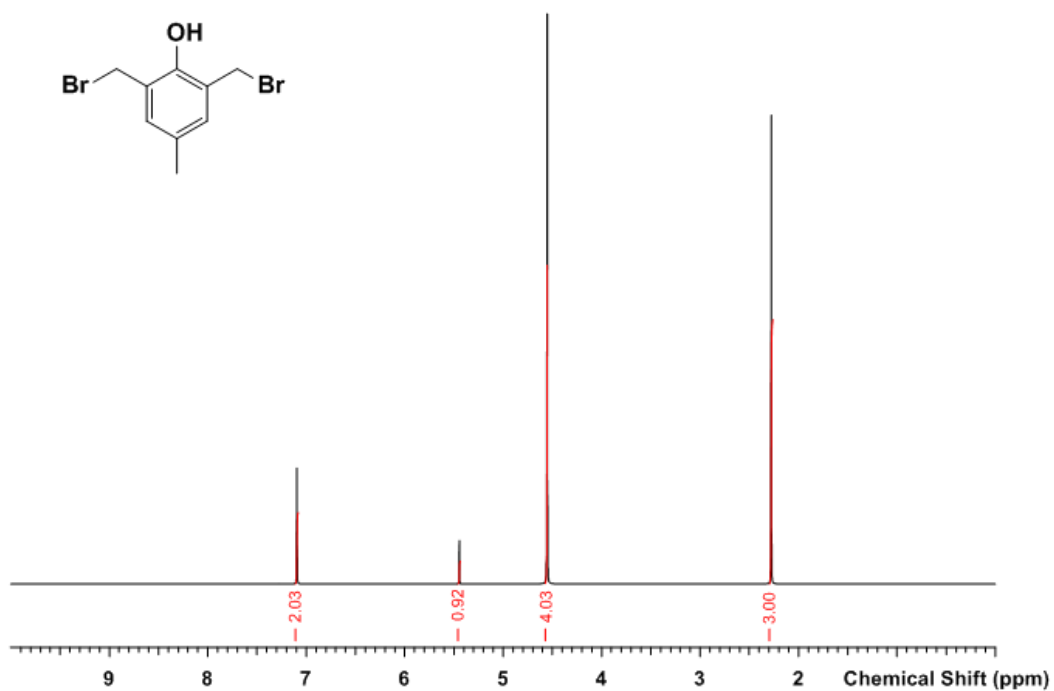


**Figure S1.** <sup>1</sup>H-NMR spectrum of compound **1** in CDCl<sub>3</sub> at 25 °C.

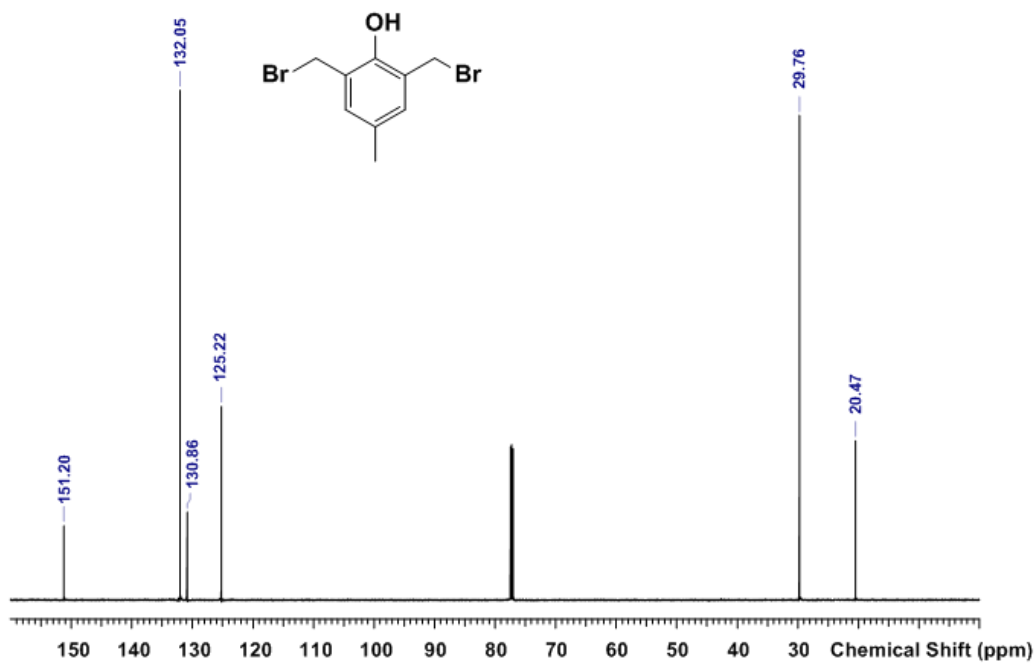


**Figure S2.** <sup>13</sup>C-NMR spectrum of compound **1** in CDCl<sub>3</sub> at 25 °C.

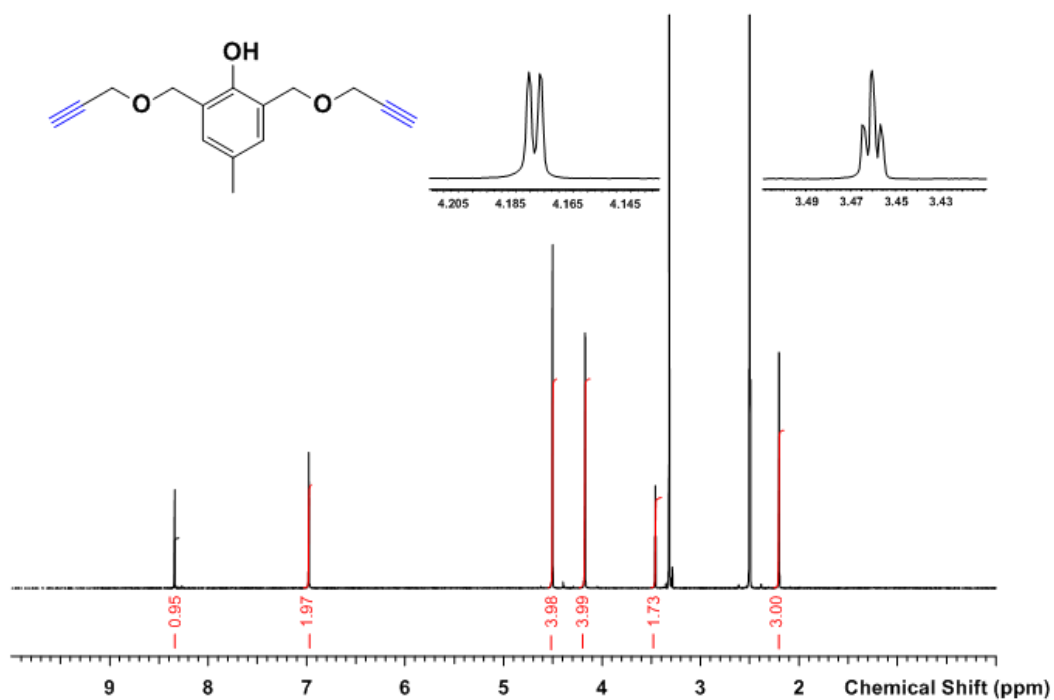


**Figure S3.** <sup>1</sup>H-NMR spectrum of compound 2 in DMSO-d<sub>6</sub> at 25 °C.

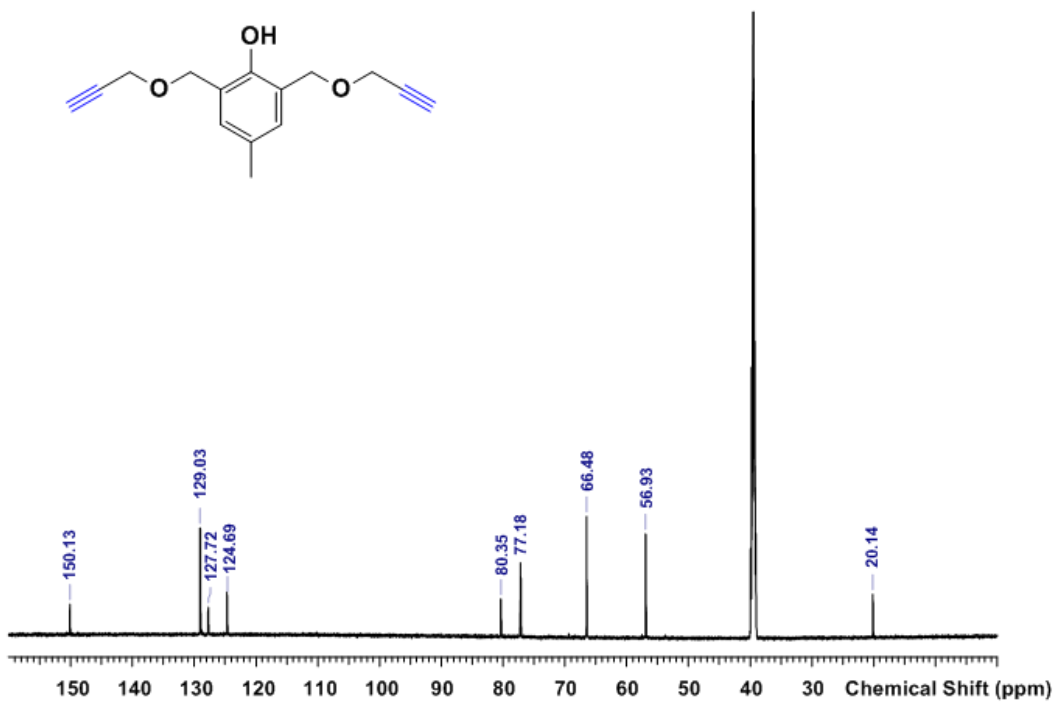


**Figure S4.** <sup>13</sup>C-NMR spectrum of compound 2 in DMSO-d<sub>6</sub> at 25 °C.

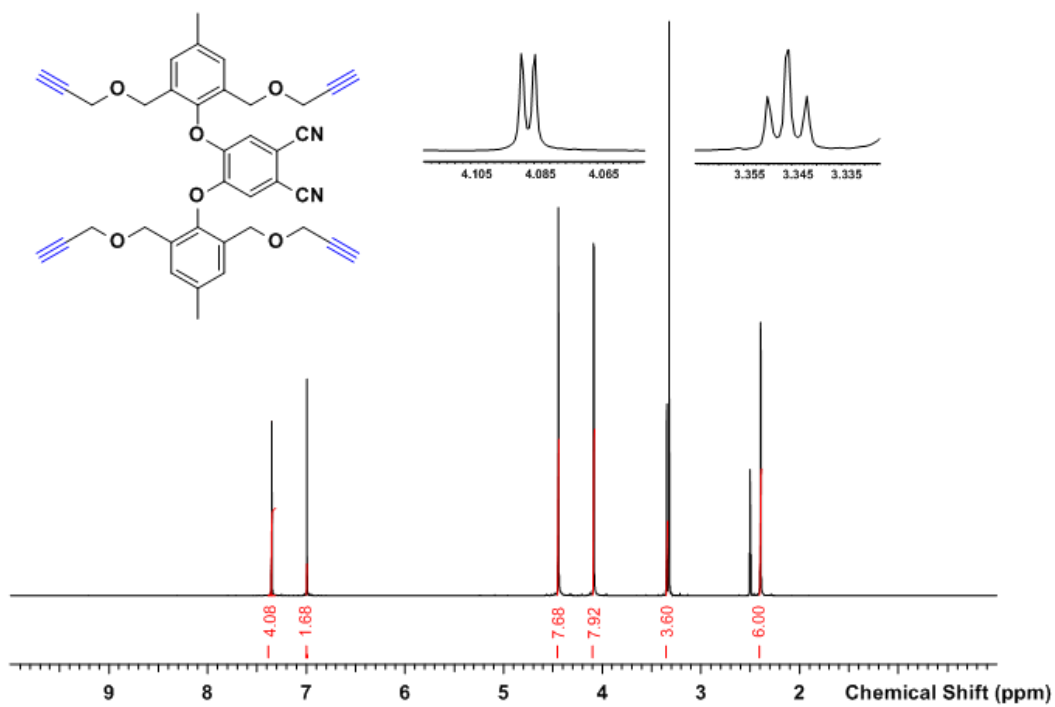


Figure S5. <sup>1</sup>H-NMR spectrum of compound 3 in DMSO-d<sub>6</sub> at 25 °C.

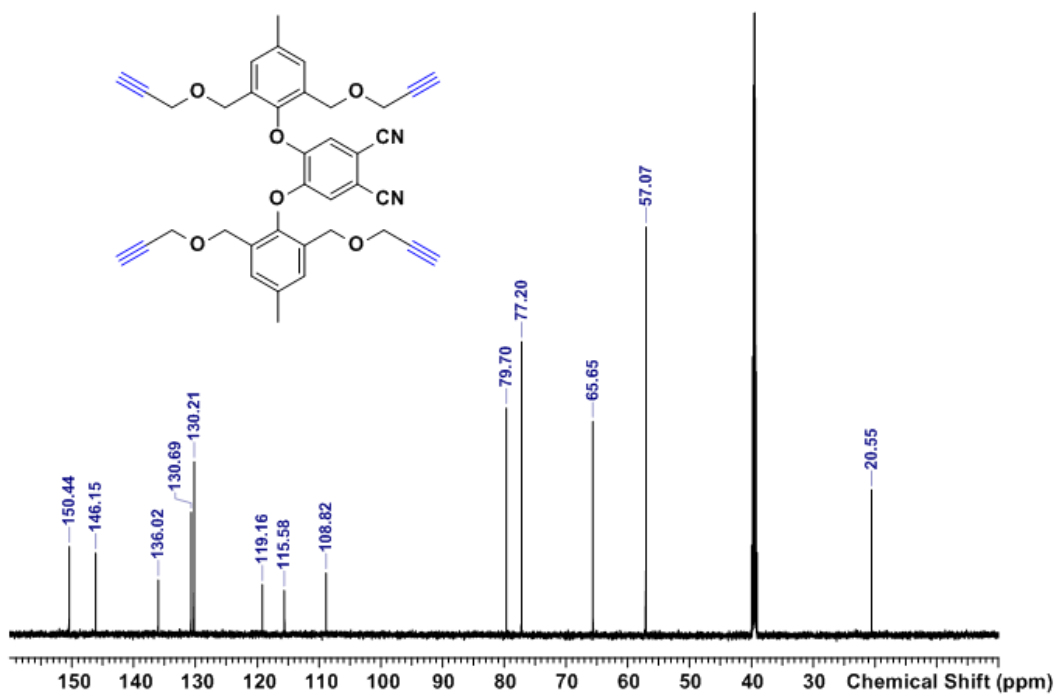
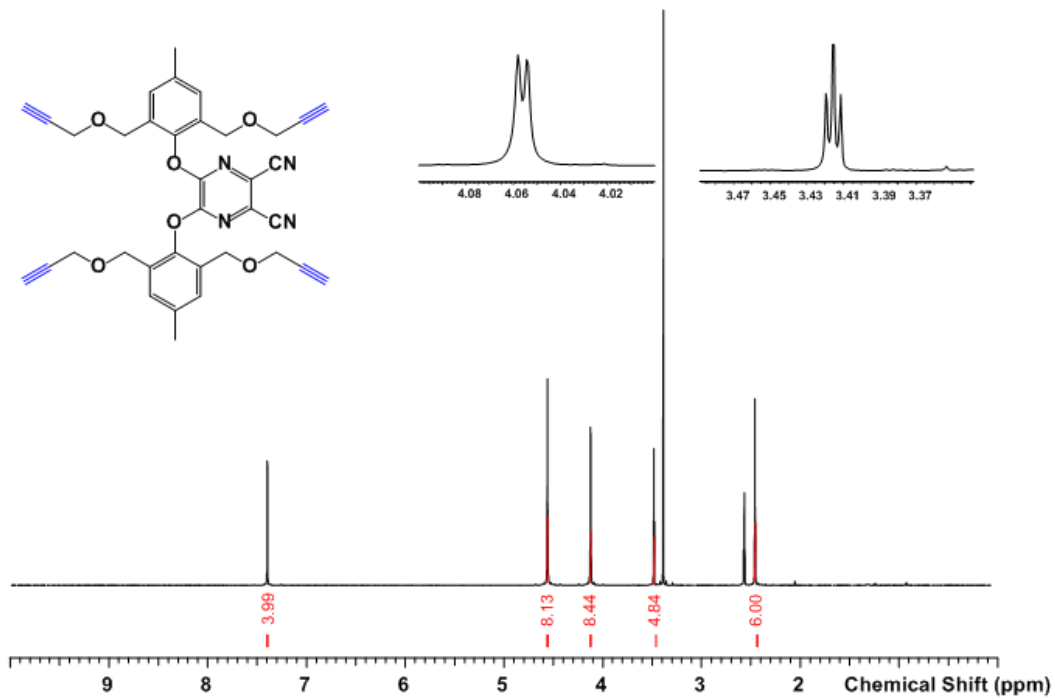
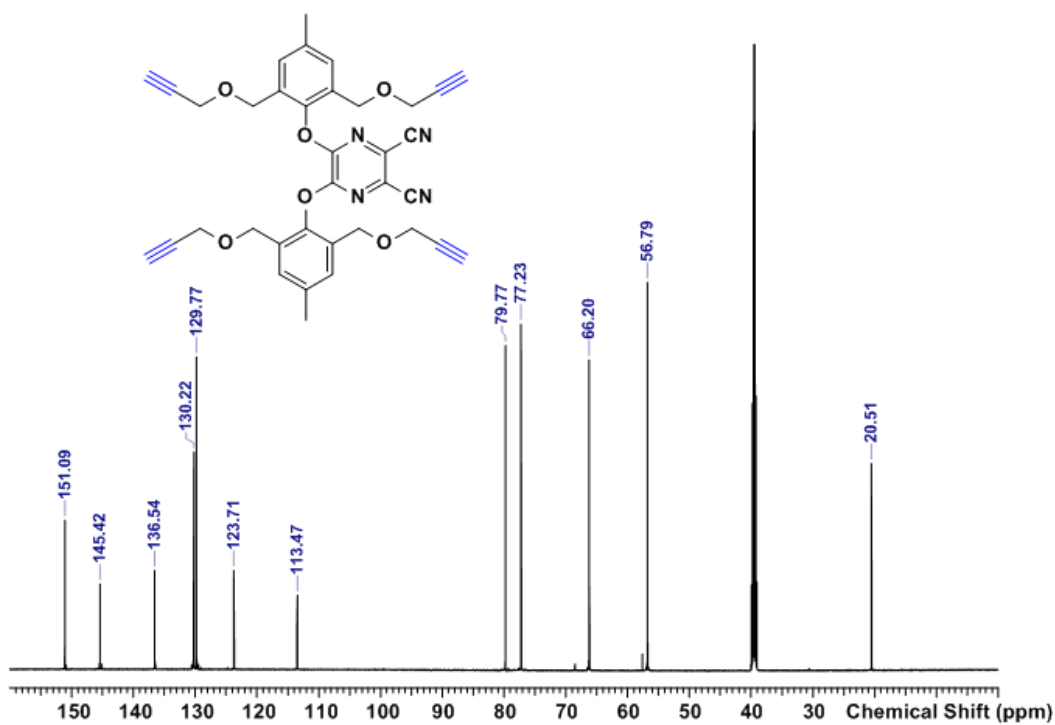


Figure S6. <sup>13</sup>C-NMR spectrum of compound 3 in DMSO-d<sub>6</sub> at 25 °C.



**Figure S7.**  $^1\text{H-NMR}$  spectrum of compound **4** in  $\text{DMSO-d}_6$  at  $25\text{ }^\circ\text{C}$ .



**Figure S8.**  $^{13}\text{C-NMR}$  spectrum of compound **4** in  $\text{DMSO-d}_6$  at  $25\text{ }^\circ\text{C}$ .

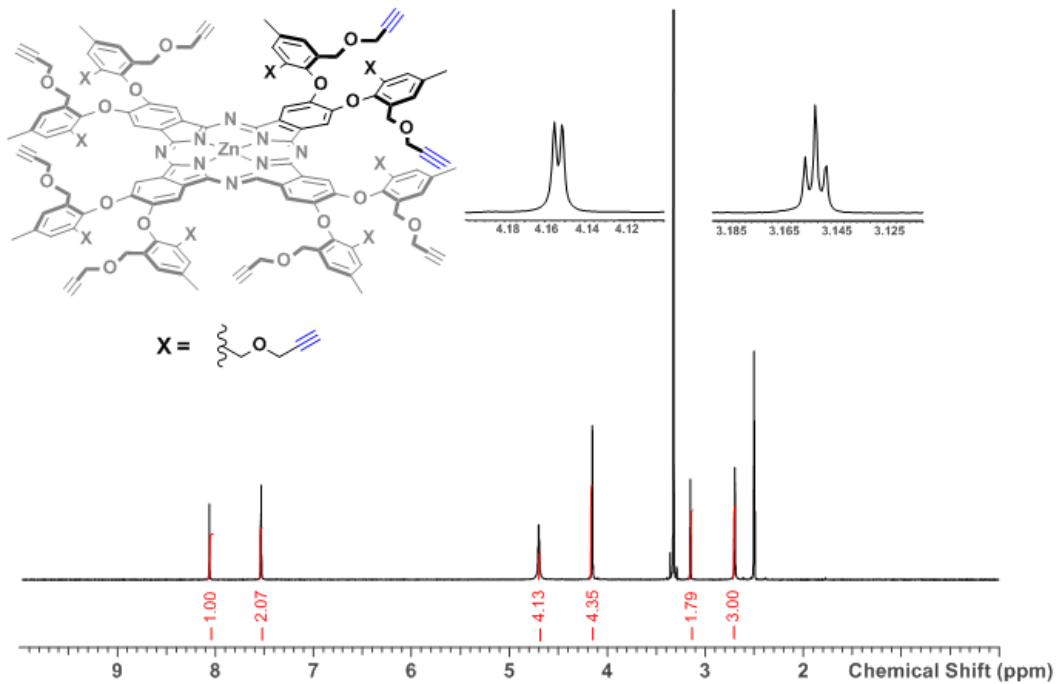


**Figure S9.**  $^1\text{H-NMR}$  spectrum of **Pc1** in DMSO- $d_6$  at 25 °C.

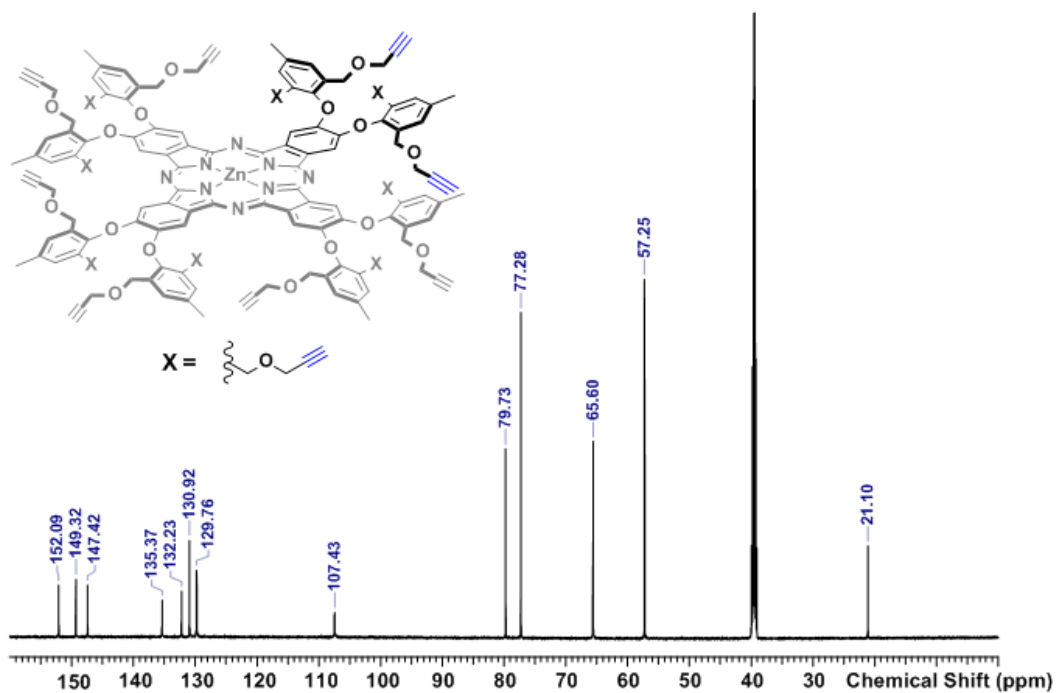


**Figure S10.**  $^{13}\text{C-NMR}$  spectrum of **Pc1** in DMSO- $d_6$  at 25 °C.

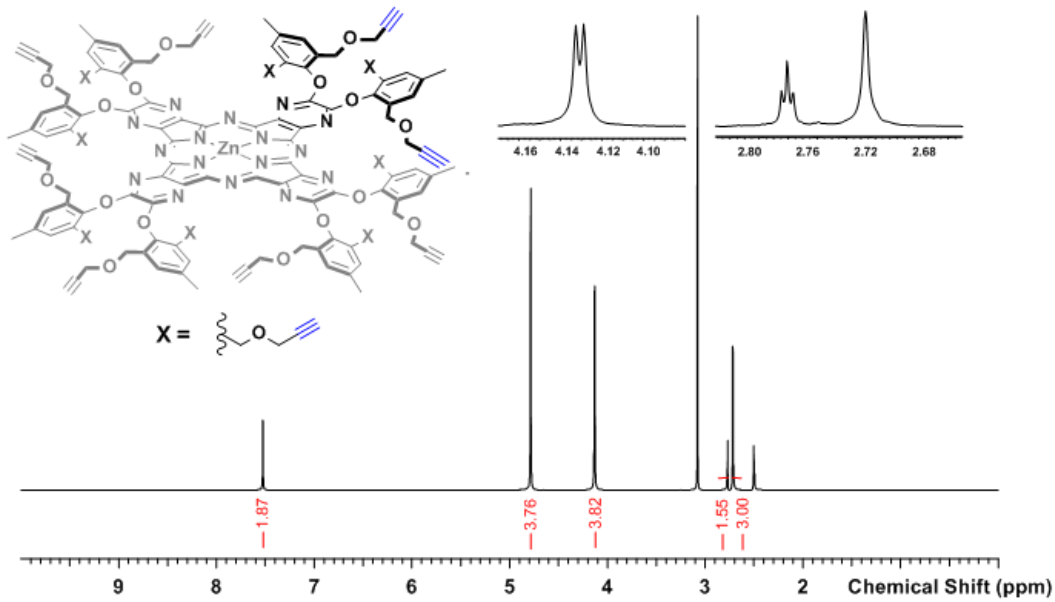


**Figure S11.**  $^1\text{H-NMR}$  spectrum of **AzaPc1** in  $\text{DMSO-d}_6$  at  $75\text{ }^\circ\text{C}$ .

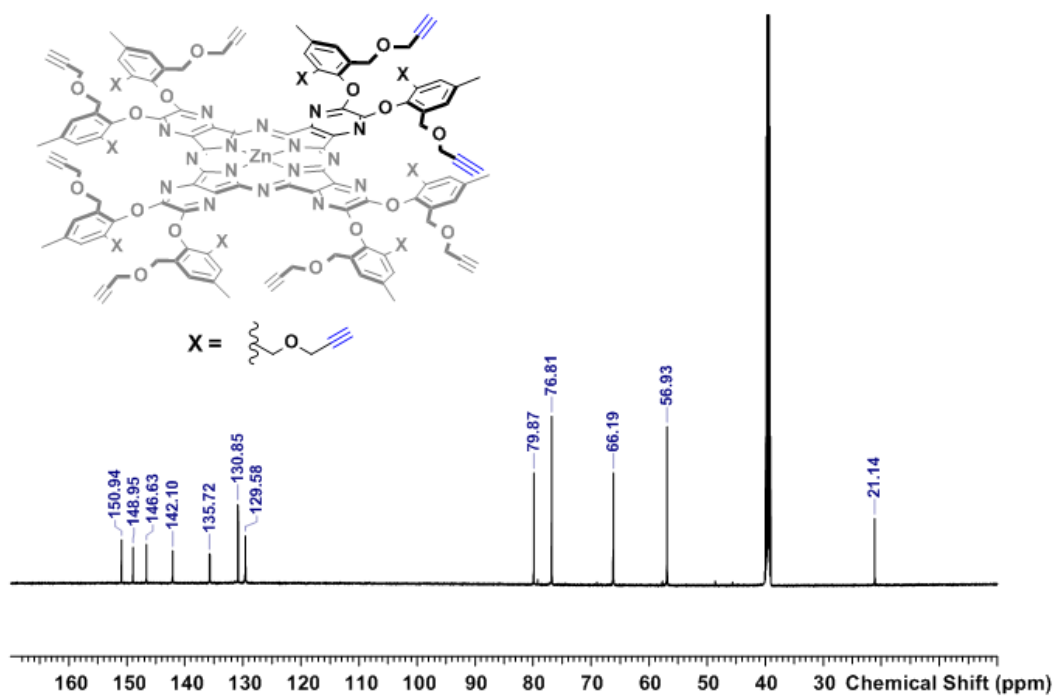


**Figure S12.**  $^{13}\text{C-NMR}$  spectrum of **AzaPc1** in  $\text{DMSO-d}_6$  at  $25\text{ }^\circ\text{C}$ .

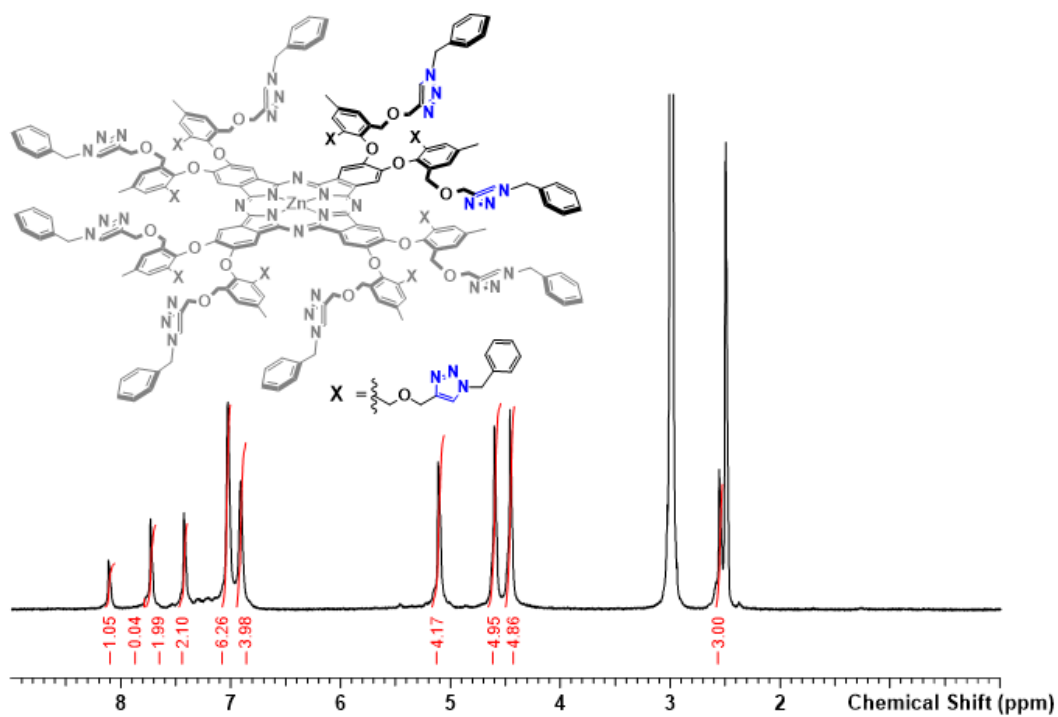


**Figure S13.**  $^1\text{H-NMR}$  spectrum of Pc2 in DMSO- $\text{d}_6$  at 25 °C.

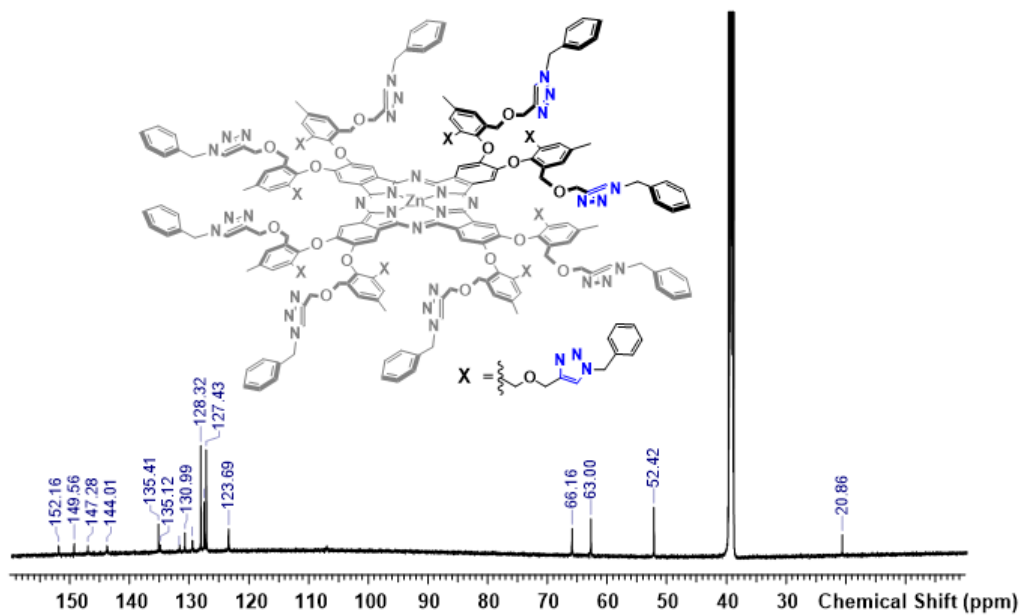


**Figure S14.**  $^{13}\text{C-NMR}$  spectrum of Pc2 in DMSO- $\text{d}_6$  at 25 °C.

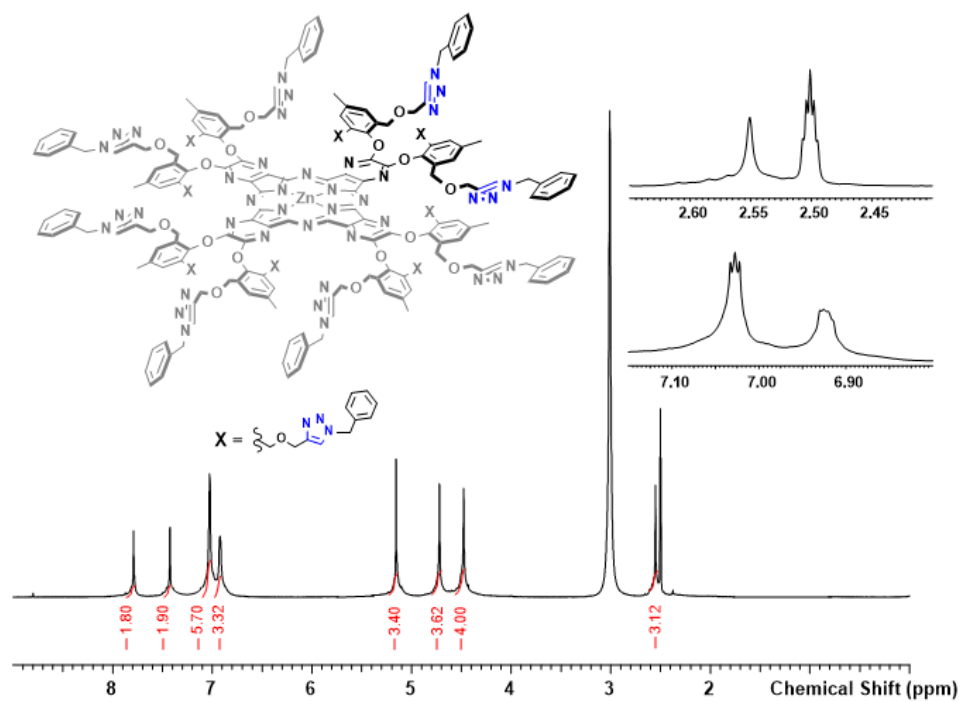


Figure S15.  $^1\text{H-NMR}$  spectrum of AzaPc2 in DMSO- $d_6$  at 25 °C.

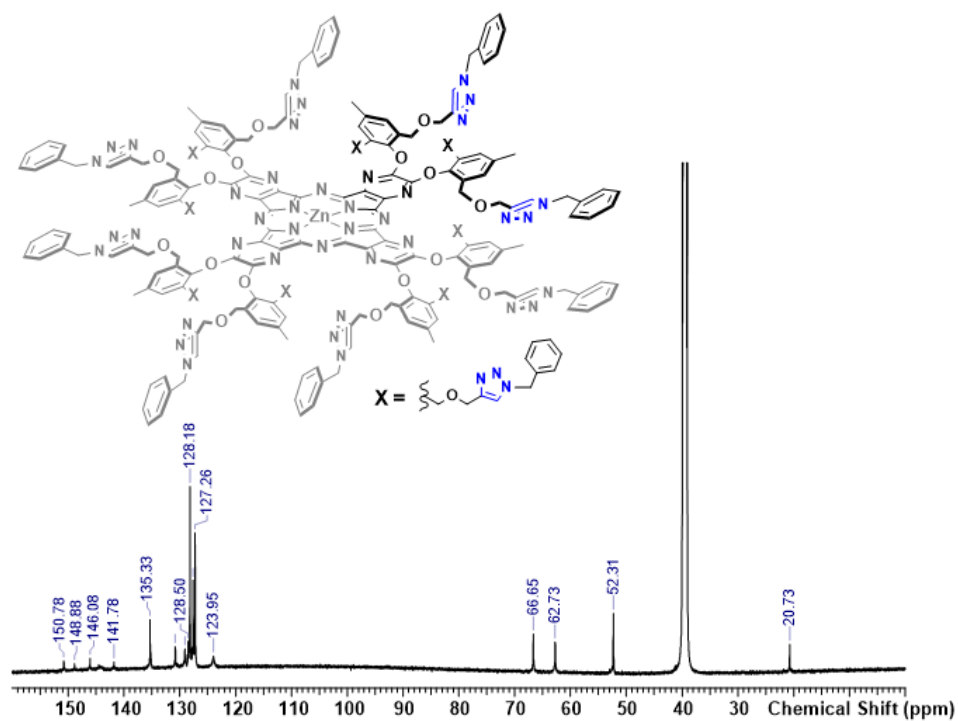
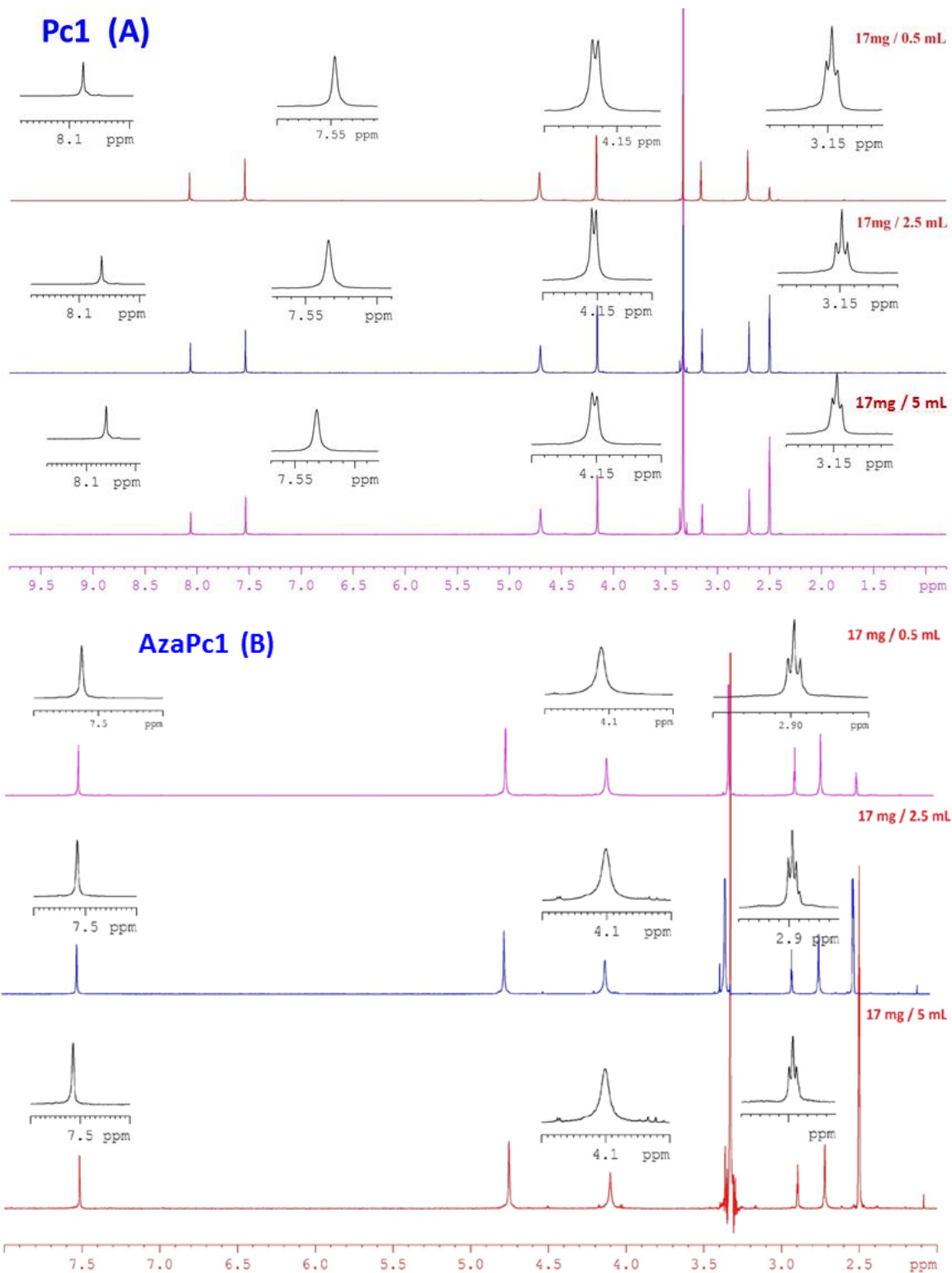
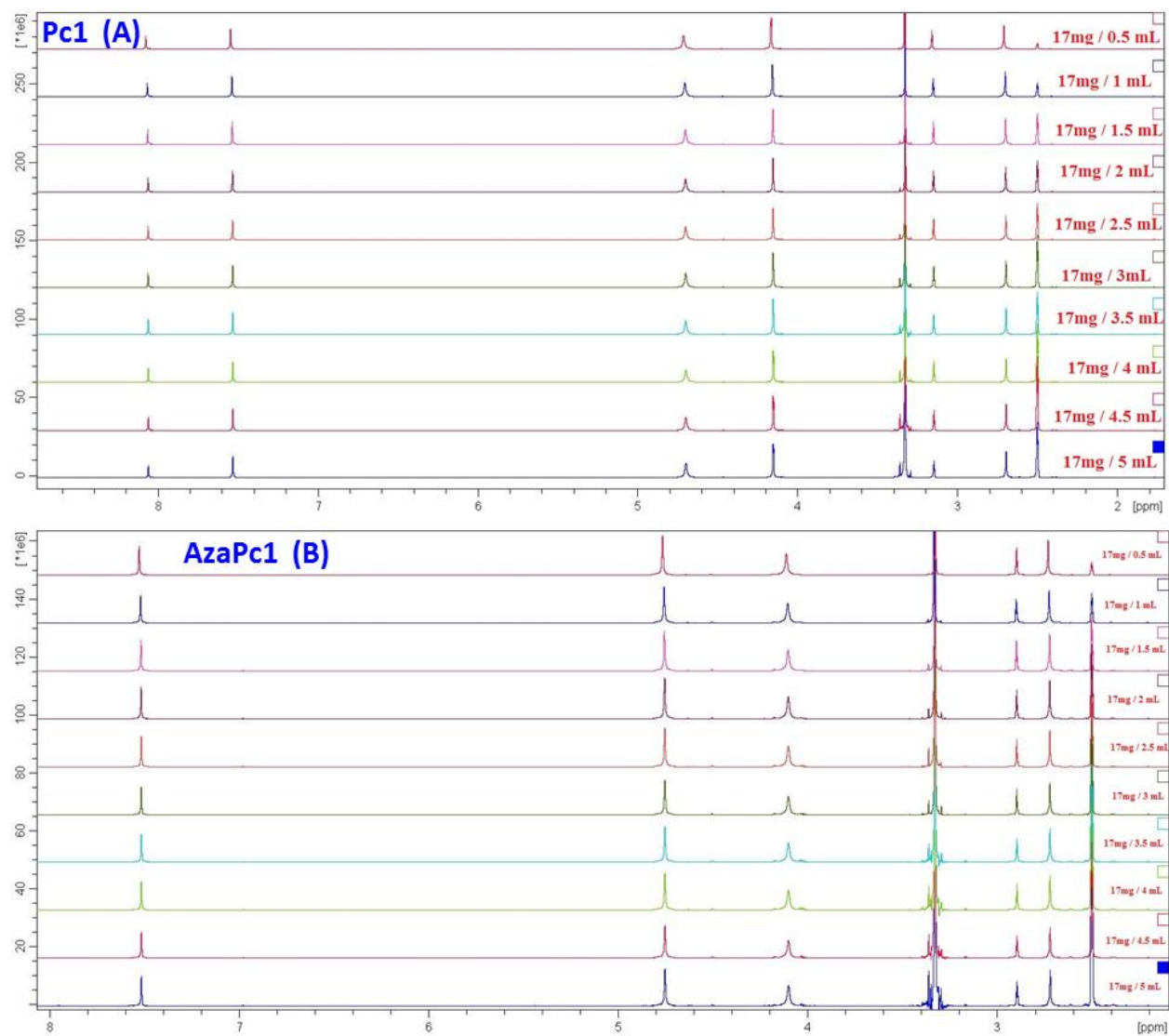


Figure S16.  $^{13}\text{C-NMR}$  spectrum of AzaPc2 in DMSO- $d_6$  at 25 °C.



**Figure S17.**  $^1\text{H}$  NMR spectrum of **Pc1** (A) and **AzaPc1** (B) in  $\text{DMSO-d}_6$  at three different concentrations (13.5, 2.69 and 1.35 mM).



**Figure S18.** <sup>1</sup>H NMR spectra of **Pc1** (A) and **AzaPc1** (B) in DMSO-d<sub>6</sub>, measured at variable concentration ranging from 13.5 mM to 1.3 mM.

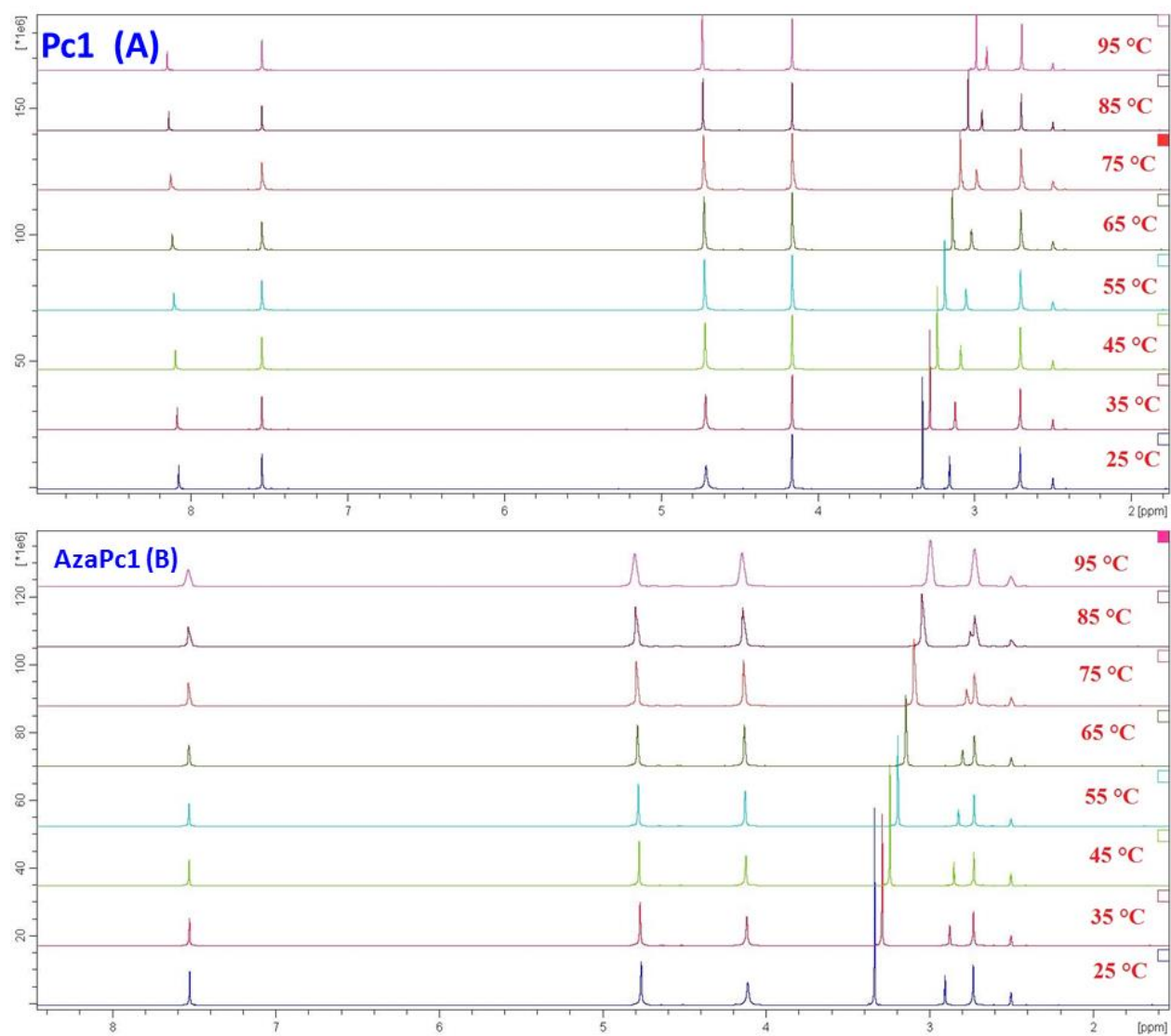


**Figure S19.** <sup>1</sup>H NMR spectra of **Pc1 (A)** and **AzaPc1 (B)** measured at variable temperature (25-95 °C) in DMSO-d<sub>6</sub>.

Mass spectra  
MALDI-TOF-MS.

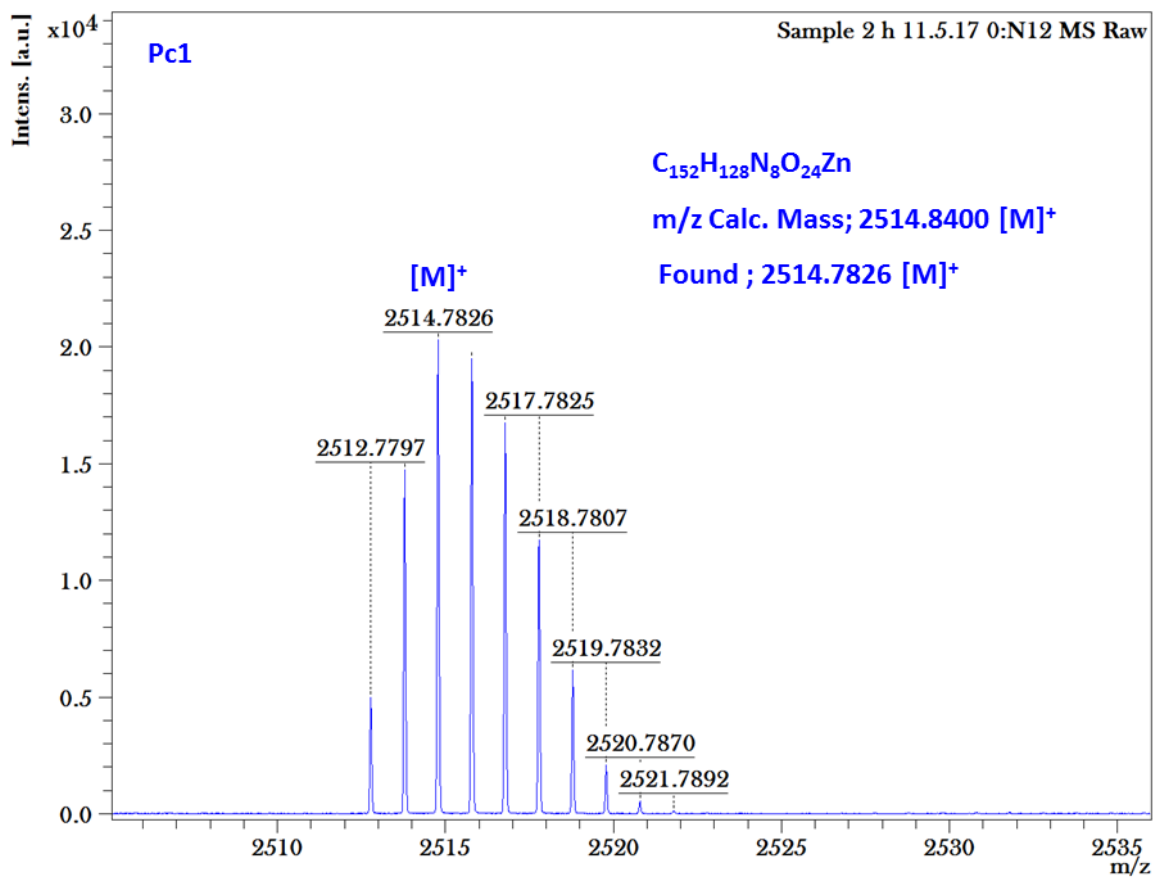
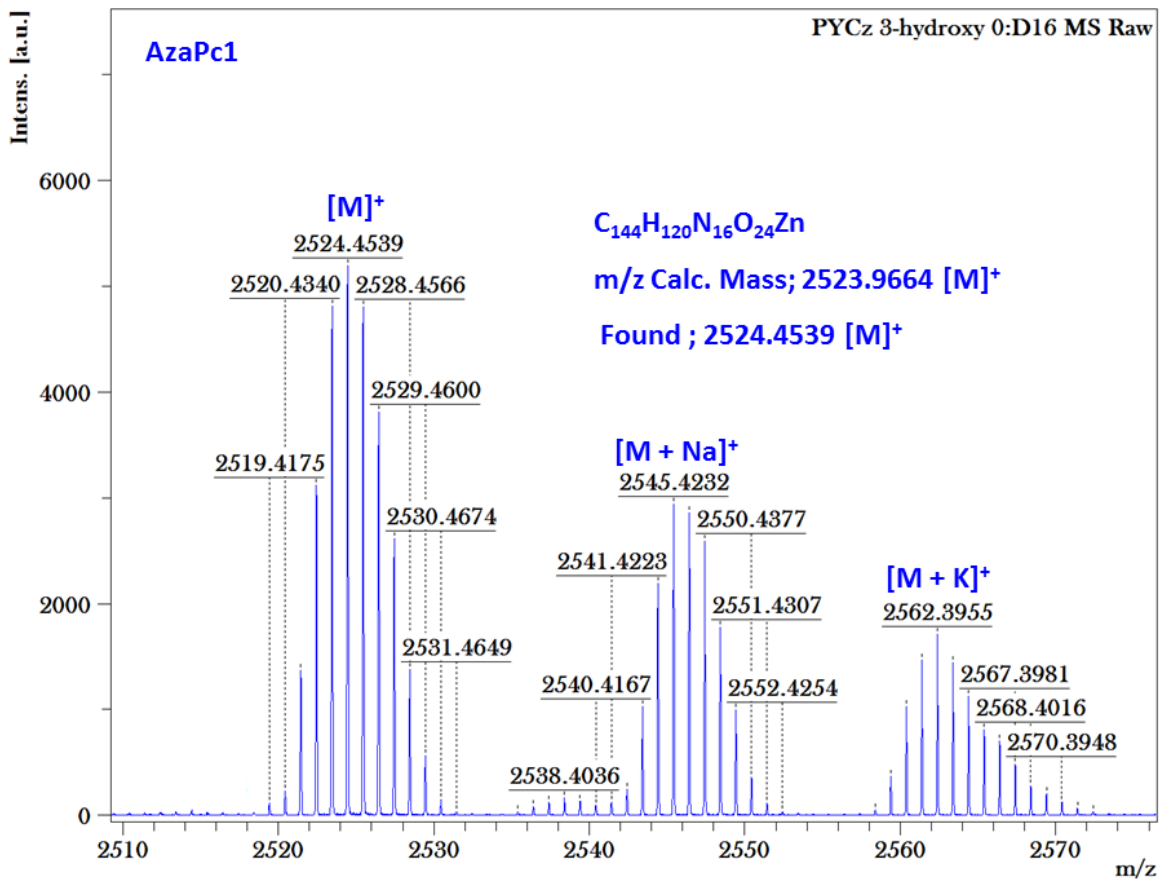


Figure S20. MALDI-TOF spectrum of Pc1.



**Figure S21.** MALDI-TOF spectrum of **AzaPc1**.

ESI-MS Spectra.

HRMS-DiBromo-re-omass4@0.01amu #4 RT: 0.44 AV: 1 NL: 9.77E5  
T: + c EI Full ms [259.50-320.50]

Compound 1

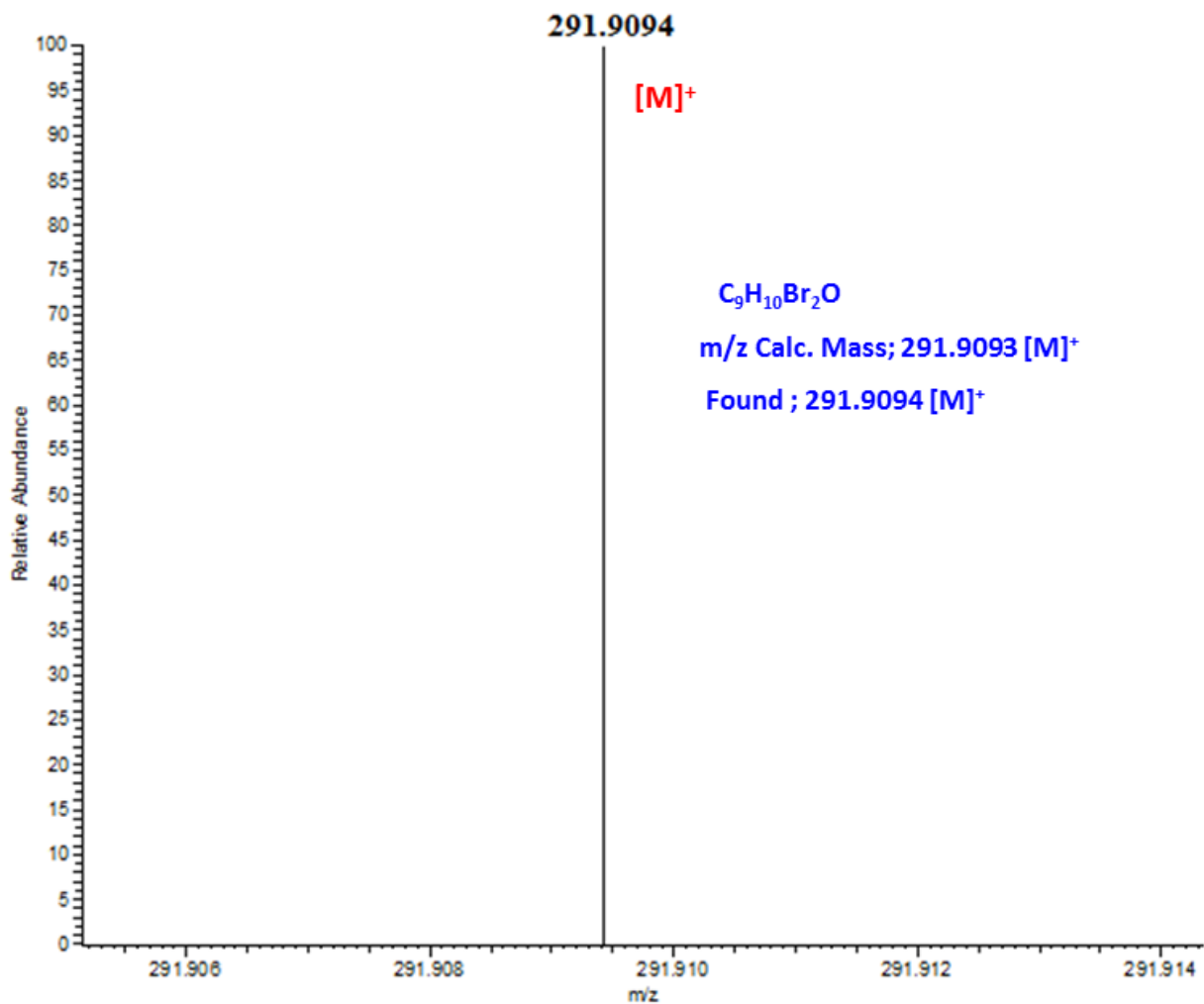


Figure S22. ESI-MS-QTOF spectrum of compound 1.

Waters Xevo G2-S QToF  
PROJECT: GS 01/03

DiALKYNE\_HRMS 11 (0.133) Cm (10:13)

1: TOF MS ES+  
2.12e5

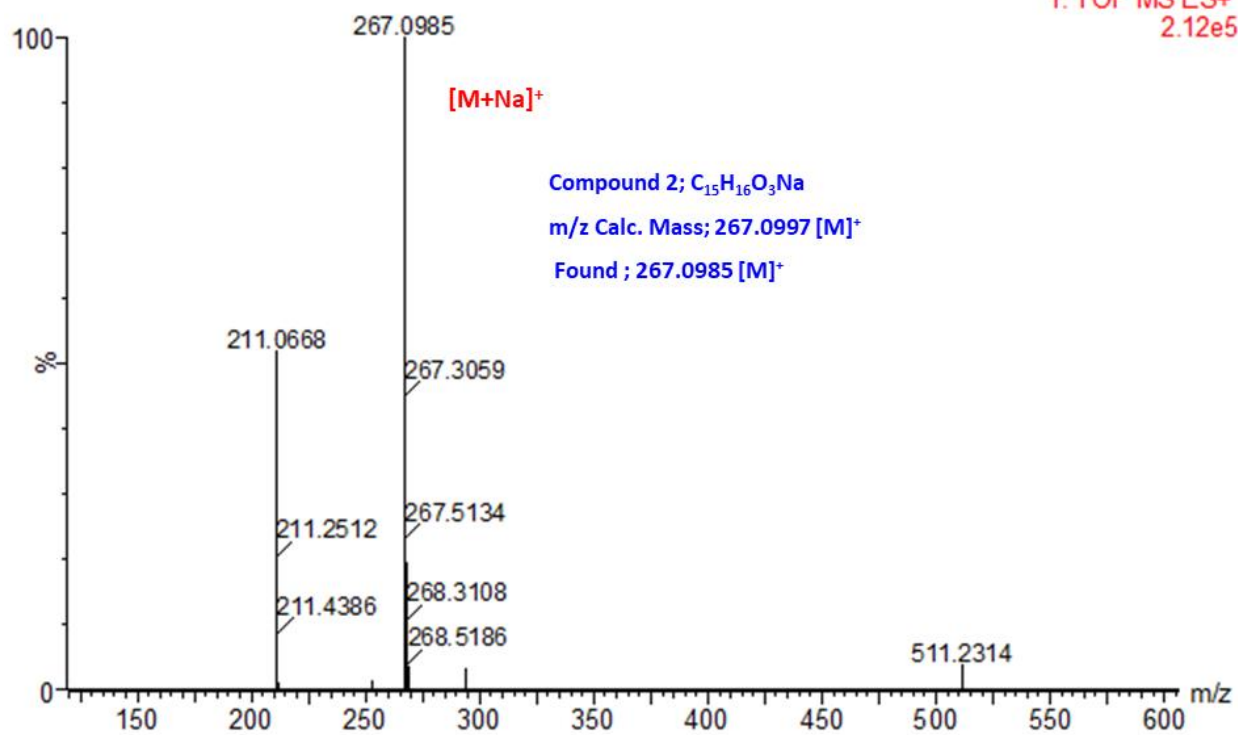
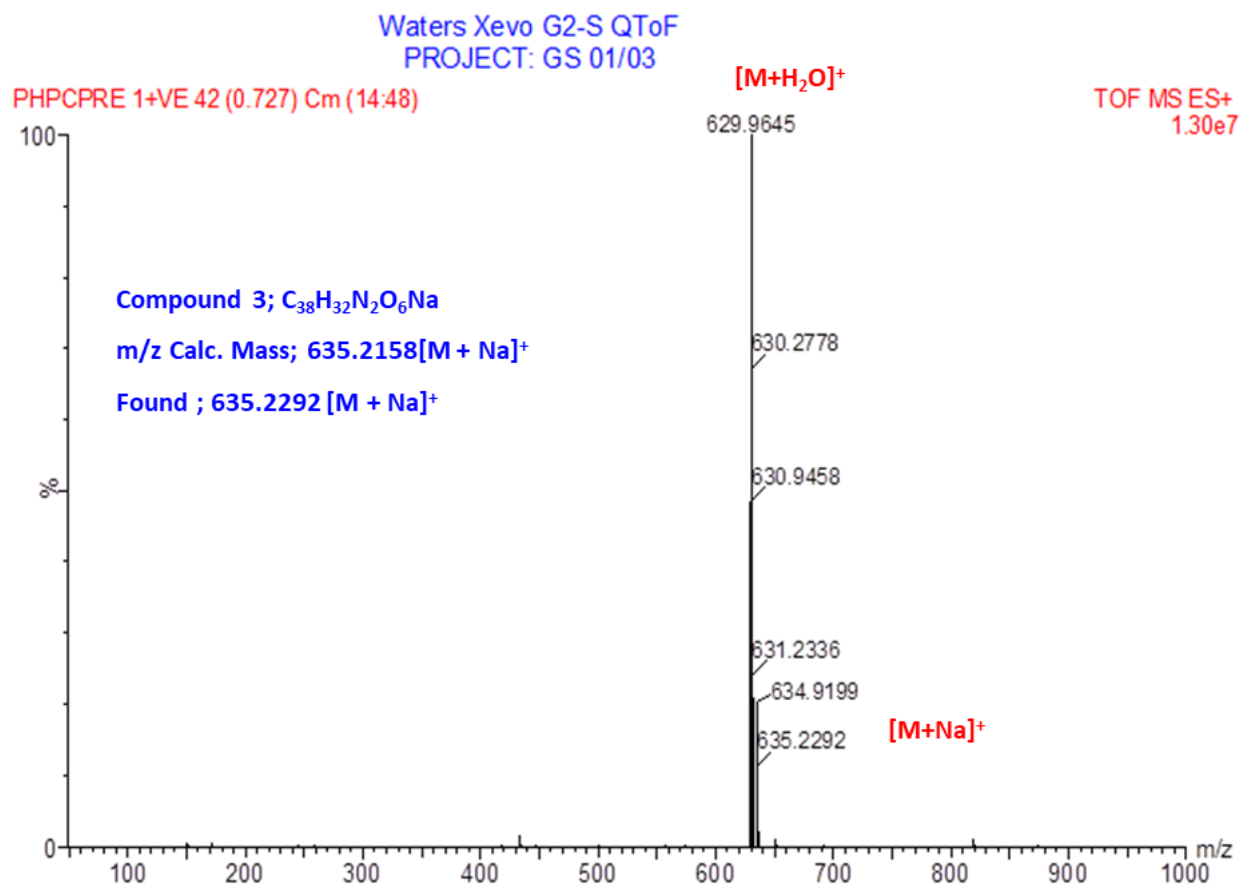
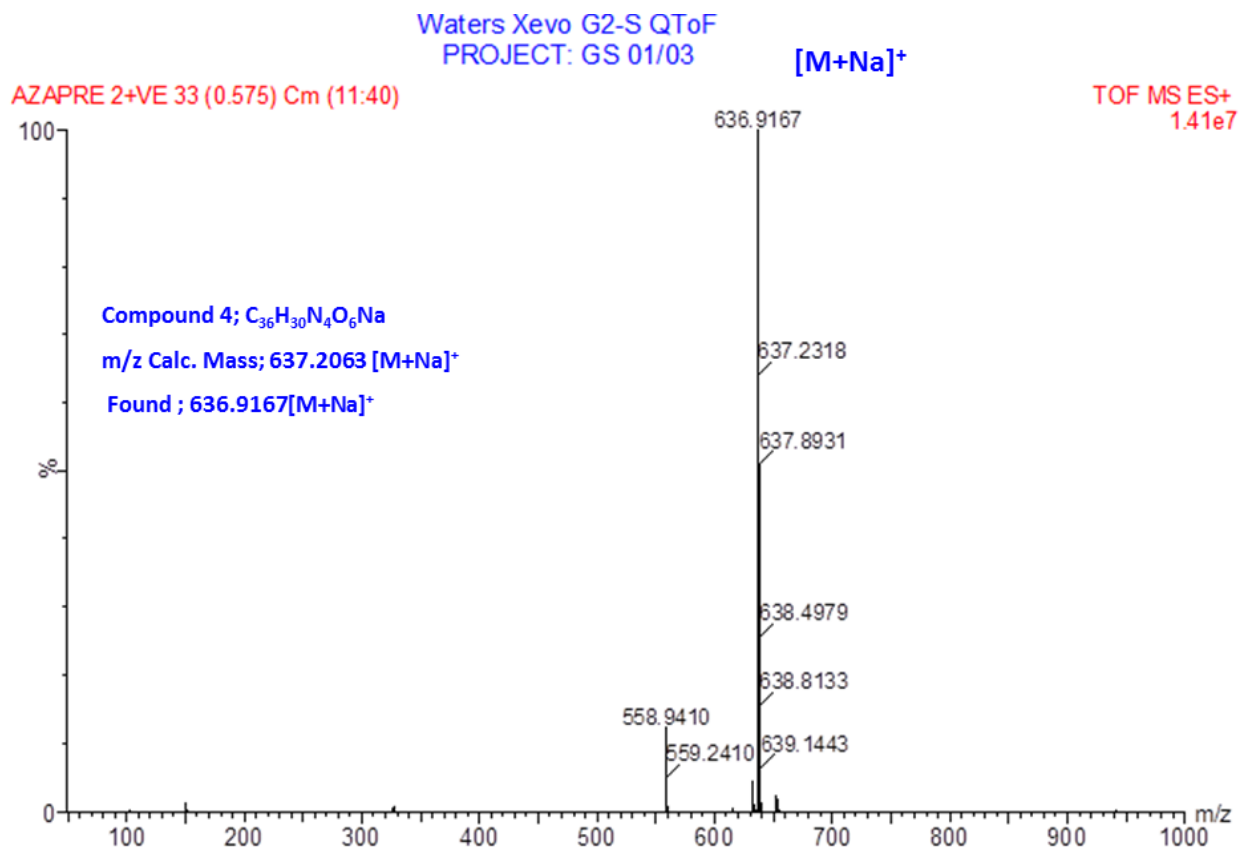


Figure S23. ESI-MS-QTOF spectrum of compound 2.



**Figure S24.** ESI-MS-QTOF spectrum of compound 3.



**Figure S25.** ESI-MS-QTOF spectrum of compound 4.

Pc2

Waters Xevo G2-S QToF  
PROJECT: GS 01/03

PHPCBENZ+VE 12 (0.220) Cm (4:24)

TOF MS ES+  
5.24e4

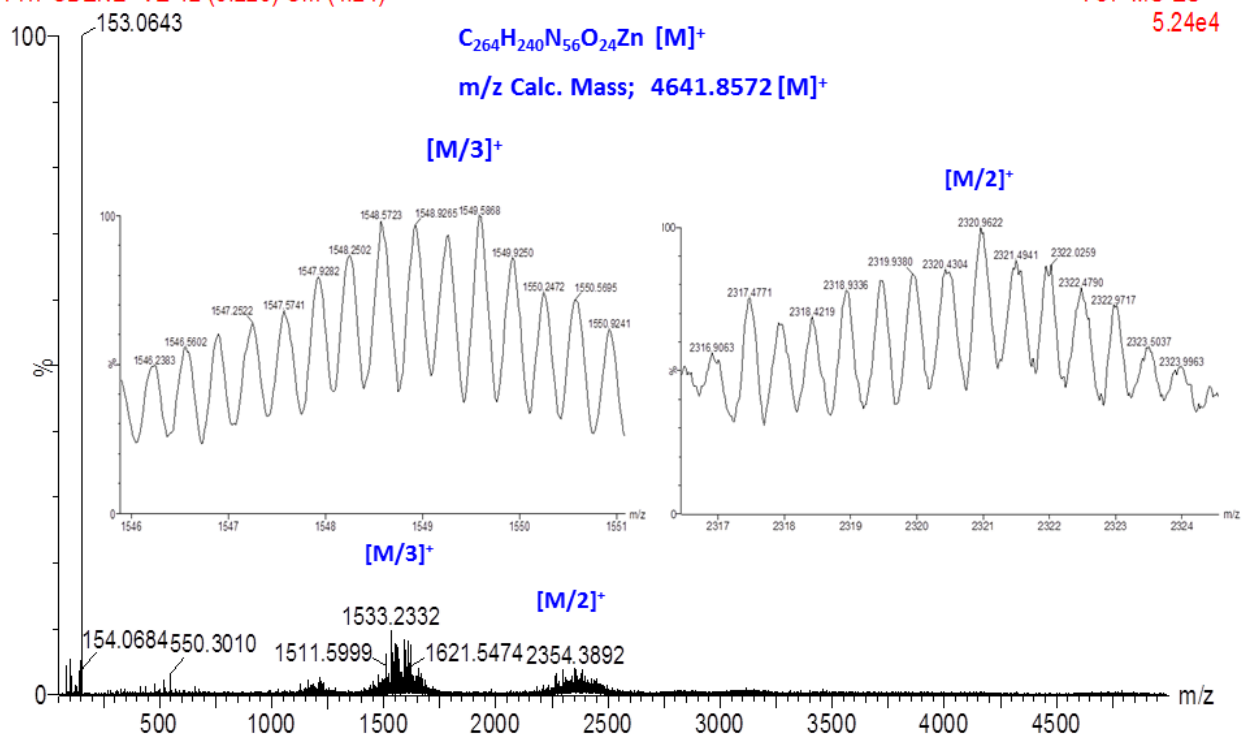
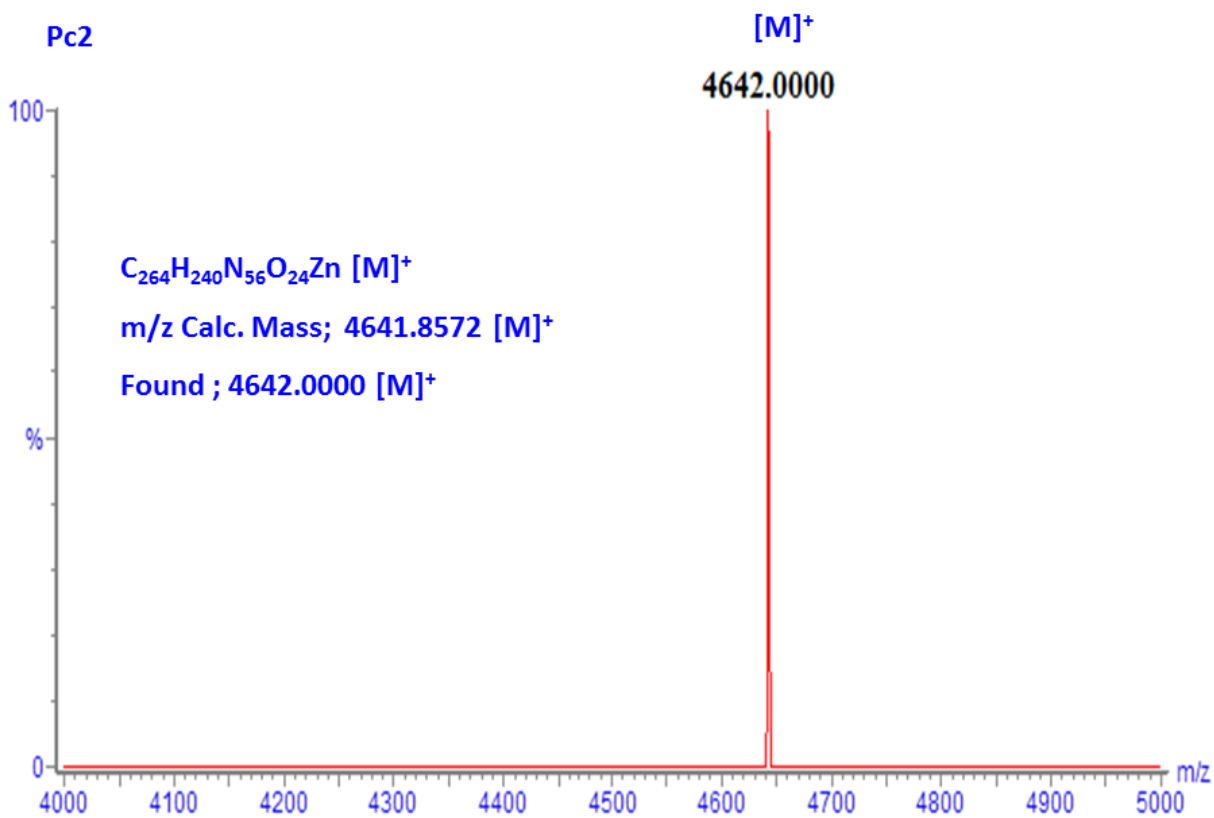
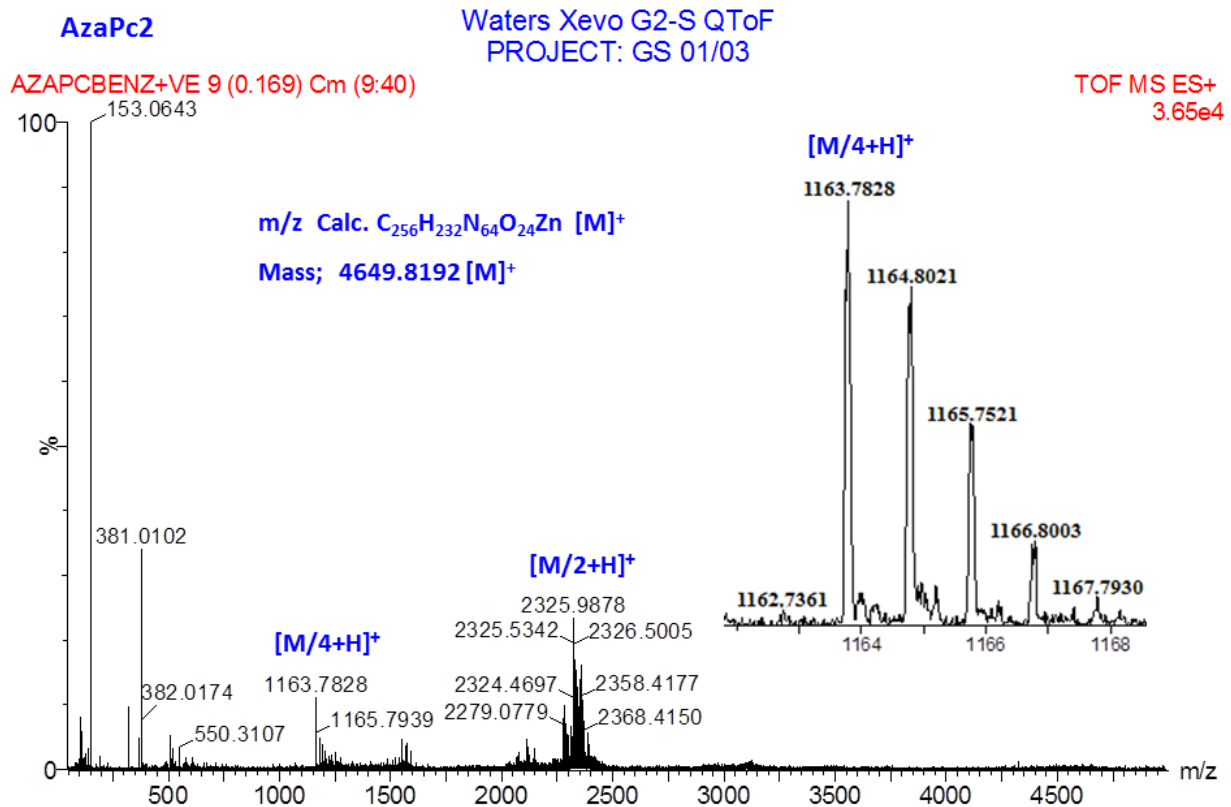


Figure S26. ESI-MS-QTOF spectrum of Pc2.



**Figure S27.** Deconvoluted HRMS (ESI) spectrum of **Pc2**.



**Figure S28.** ESI-MS-QTOF spectrum of **AzaPc2**.

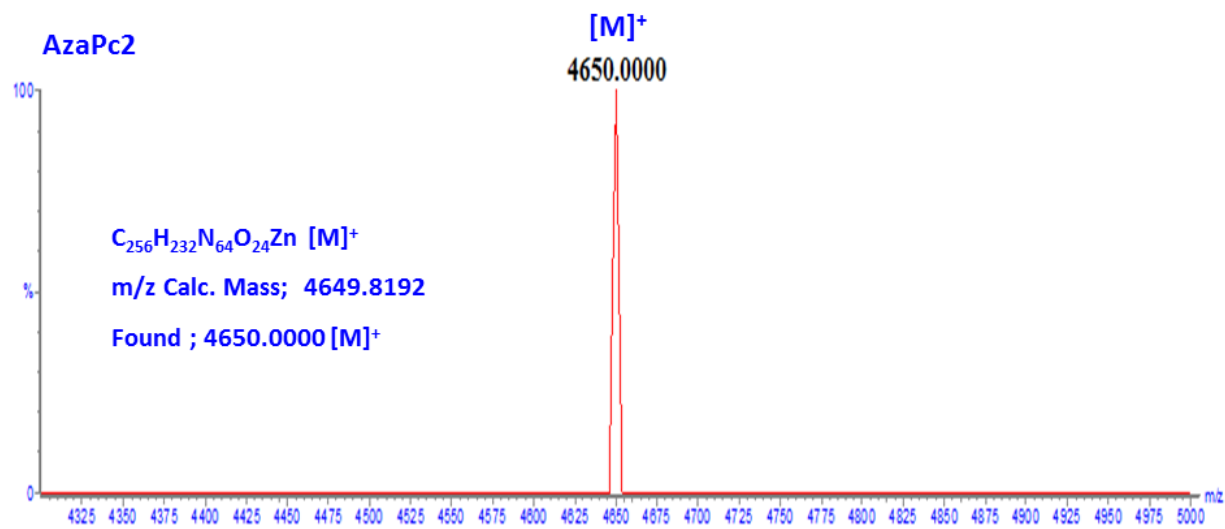


**Figure S29.** Deconvoluted HRMS (ESI) spectrum of **AzaPc2**.

## Result and discussion

### Photophysical characterization

#### Ground state electronic absorption spectra of Pc1/AzaPc1

The electronic absorption which is measured by UV-Vis spectroscopy is one of the best spectroscopic techniques for determination of Pcs formation. This spectroscopy is a useful method for characterization of Pc compounds. Generally, two absorption bands are observed for Pc structures in their electronic absorption spectra. One of them which is known as Q, is observed at around 600-750 nm due to the  $\pi \rightarrow \pi^*$  transitions from the highest occupied molecular orbital (HOMO) to the lowest unoccupied molecular orbital (LUMO) of the Pc ring, while the other one (B, Soret band) is observed in the ultraviolet region of spectrum at around 300-450 nm arising from deeper  $\pi$  levels  $\rightarrow$  LUMO.<sup>[9]</sup> The ground state electronic absorption spectra of the studied novel Pcs were measured in DMF solution. The UV-Vis spectra of these molecular structures are supplied Figure S30.

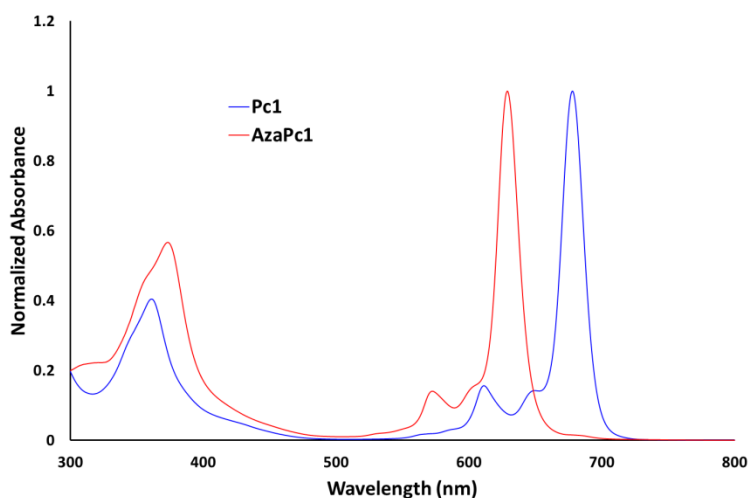


**Figure S30.** Electronic absorption spectra of **Pc1/AzaPc1** in DMF.

Their ground state electronic absorption spectra showed monomeric behavior evidenced by a single (narrow) Q band absorptions which is typical for metallated complexes.<sup>[9]</sup> The Q bands were observed around at 680 nm for **Pc1** in DMF (Table S1).

The observed red spectral shifts are typical for Pc molecules with substituents at the non-peripheral positions and have been explained to be due to linear combinations of the atomic

orbitals (LCAO) coefficients at the non-peripheral positions of the HOMO being greater than those at the peripheral positions.<sup>[10]</sup> As a result, the HOMO level is destabilized more at the non-peripheral site than it is at the peripheral one. Essentially, the energy gap ( $\Delta E$ ) between the HOMO and LUMO becomes smaller, resulting in a bathochromic shift. The 49 nm blue shift for **AzaPc1** is caused by the additional nitrogen atoms instead of CH groups in the Pc macrocyclic system. The B-bands are broad due to the superimposition of the B1 and B2 bands in the 340 to 380 nm region.

### Aggregation studies

Macrocyclic Pcs generate high aggregation tendencies due to the intermolecular interactions that take place between their 18  $\pi$ -electrons. Accordingly, this self-association process would minimize their solubility in most solvent systems and therefore affects their spectroscopic, photophysical, photochemical and electrochemical properties. Generally, aggregation is highly dependent on the concentration, temperature, nature of the substituents and/or their position and orientation with respect to the Pc skeleton, nature of the solvent media and the central metal ion in the Pc-cores.<sup>[11]</sup> Pc molecules can form two types of aggregates in dissolved system, i.e.; the H-type and J-type, depending on the nature, position and/or orientation of the substituents. In general, Pcs form H-type aggregates in solution, whereas the J-type aggregation was observed rarely for these assemblies. The formation of J-type aggregates among the Pc structures is significant since this type of aggregates is photoactive, while the H-type aggregates is not appear. The aggregation properties for all **Pc1/AzaPc1** were recorded in different organic solvents, namely; DCM, chloroform, DMF, DMSO, ethanol, methanol, THF and toluene. Interestingly, no aggregation for these assemblies was observed in all organic solvents used (Figure S31).

Aggregation behaviors for **Pc1/AzaPc1** were also investigated in DMF at different concentration in order to establish a suitable concentration for further photophysical and photochemical studies. The Beer-Lambert law was obeyed at concentrations ranging from  $1.0 \times 10^{-5}$  to  $1.0 \times 10^{-6}$  M. Both these cyclic derivatives did not show any aggregation within this concentration range (Figure S32).

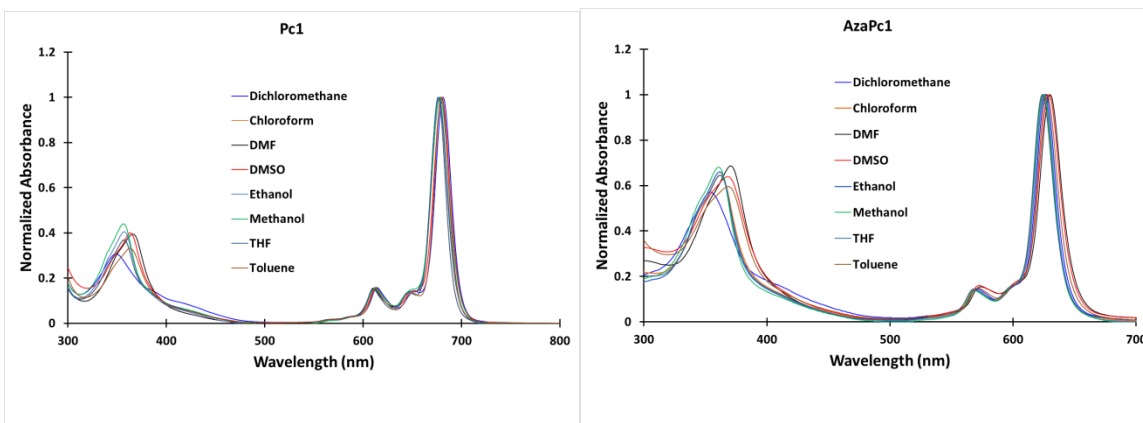


**Figure S31.** Electronic absorption spectra of **Pc1/AzaPc1** in different solvents.

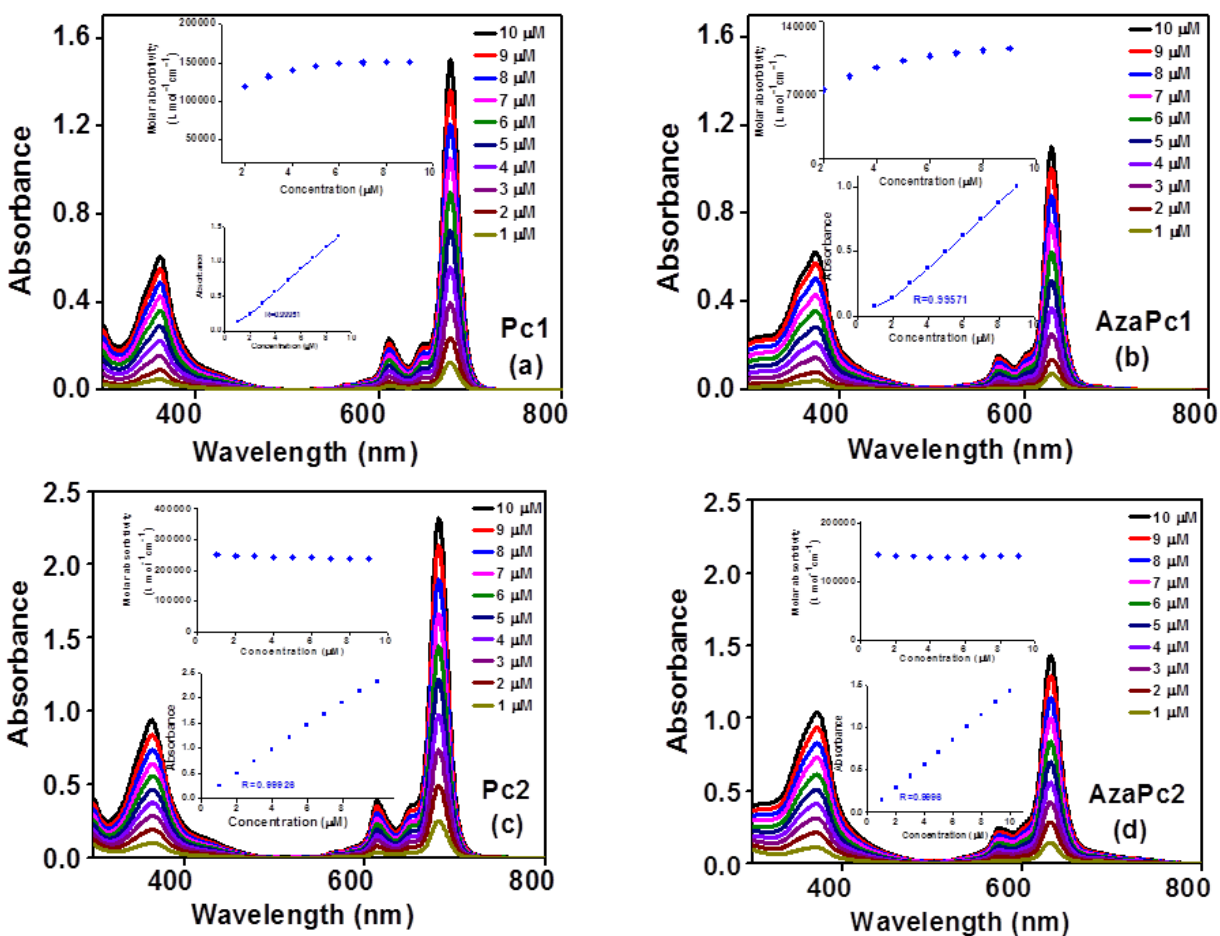


**Figure S32.** Aggregation behavior of **Pc1** (a), **AzaPc1** (b), **Pc2** (c) and **AzaPc2** (d) in DMF at different concentrations ranging from 1 to 9  $\mu\text{M}$ ; (Insets: Plot of absorbance versus concentration and other plot is dependence of the extinction coefficient at  $\lambda_{\text{max}}$  for **Pc1**, **AzaPc1**, **Pc2** and **AzaPc2**).

## Fluorescence measurements

The fluorescence behaviors of **Pc1**, **AzaPc1**, **Pc2** and **AzaPc2** were evaluated in DMF solutions. Figure S33 shows absorption, fluorescence emission and excitation spectra of these complexes. The resulted studies in DMF showed similar fluorescence behavior in DMF in which the excitation spectra were similar to the absorption spectra and both were mirror images of the fluorescence emission spectra for all studied complexes. The proximity of the wavelength of each component of the Q-band absorption to the Q band maxima of the excitation spectra for both zinc (II) complexes suggested that the nuclear configurations of the ground and excited states are similar and not affected by excitation.

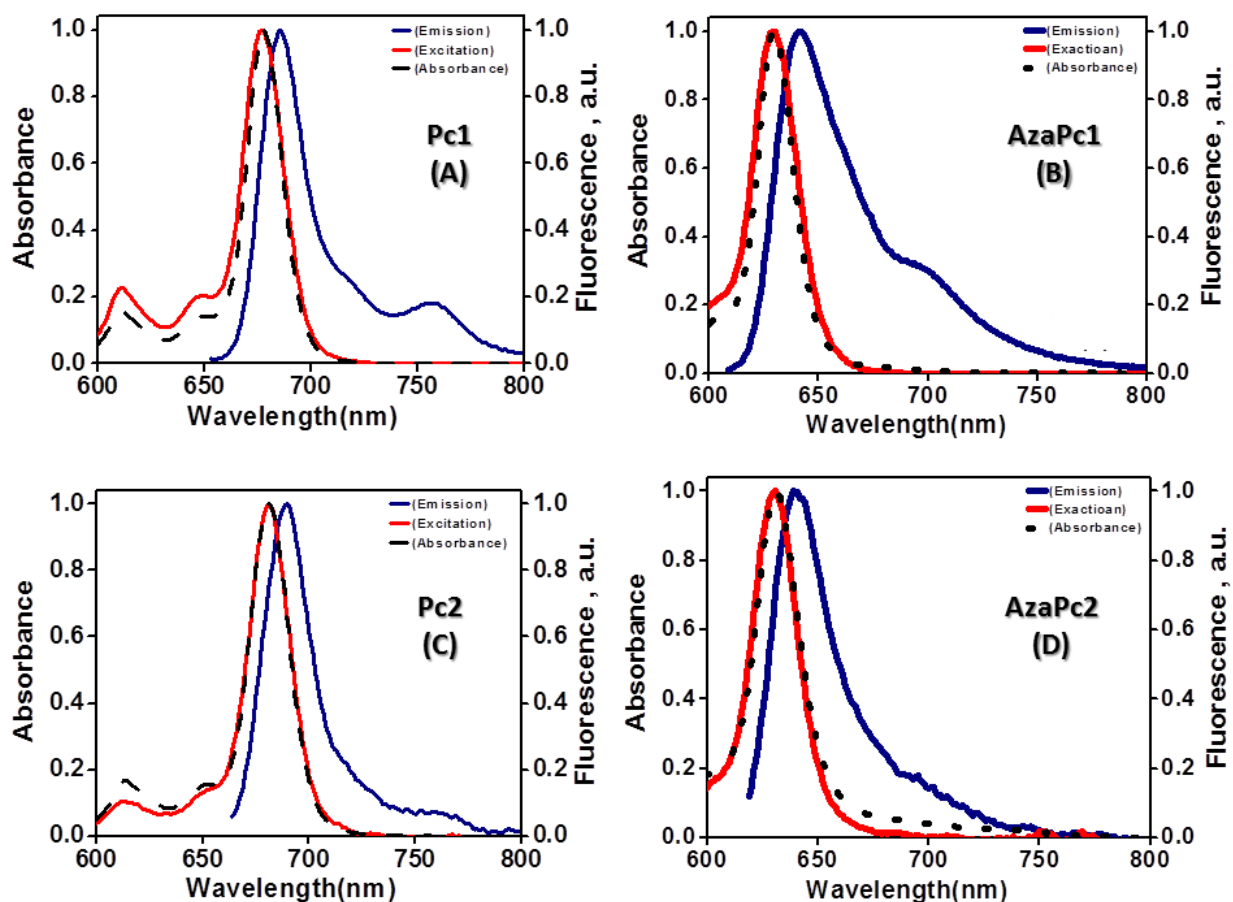


**Figure S33.** Absorption, excitation and emission spectra of **Pc1** (a), **AzaPc1** (b), **Pc2** (c) and **AzaPc2** (d) in DMF. Excitation wavelength = 678 nm for **Pc1**, 681 nm for **Pc2**, 629 nm for **AzaPc1** and 631 nm for **AzaPc2**

The excitation wavelengths were observed at 678 nm for **Pc1**, 681 nm for **Pc2**, 629 nm for **AzaPc1** and 631 nm for **AzaPc2** in DMF. The emission maxima were observed at around 683 nm for **Pc1** and **Pc2** and around 630 nm for **AzaPc1** and **AzaPc2**. The observed Stokes' shifts which are differences between the excitation and emission wavelength maxima were found between 4 and 10 nm for zinc (II) complexes (Table S1). The observed Stokes' shifts were found within the region observed for typical zinc(II) phthalocyanine complexes.<sup>[12]</sup> By following the same procedure used for **Pc1/AzaPc1** complexes, the fluorescence emission and excitation spectra of the forming **Pc2** and **AzaPc2** complexes were depicted in Figure S33C and S33D, respectively. The spectral features in terms of small Stokes' shift and the maintained mirror symmetry between the emission and excitation peaks were achieved.

## Fluorescence quantum yields and lifetimes

Fluorescence emission occurs when an orbital electron of a photosensitizer relaxes from its singlet state to ground state upon emitting a photon of light. The fluorescence quantum yield ( $\Phi_F$ ) gives the efficiency of the fluorescence process and this value is defined as the ratio of the number of photons emitted to the number of photons absorbed. The fluorescence quantum yields ( $\Phi_F$ ) were determined using established method described in literature.<sup>[4]</sup> The  $\Phi_F$  values of **Pc1/AzaPc1** were typical for those phthalocyanine compounds (Table S1). These values were found as 0.16 for **Pc1** and 0.14 for **AzaPc1** in DMF solvent system. However, the  $\Phi_F$  values were determined to be 0.1 for both **Pc2** and **AzaPc2** complexes which were found to be slightly lower than their corresponding building blocks, **Pc1** and **AzaPc1**.

Further, fluorescence lifetime ( $\tau_F$ ) refers to the average time for a molecule stays in its excited state before returns to its ground state by emitting.<sup>[13]</sup> In this study, the fluorescence lifetime values of studied **Pc1/AzaPc1** were determined by using time correlated single photon counting (TCSPC) method. All time-resolved fluorescence studies were carried out in DMF and the fluorescence decays of the macrocycles were concluded in mono exponential curves (Figure S34). The fluorescence lifetime values were found as 3.30 ns for **Pc1**, 2.90 ns for **Pc2**, 2.46 ns for **AzaPc1** and 2.45 ns for **AzaPc2** (Table S1).

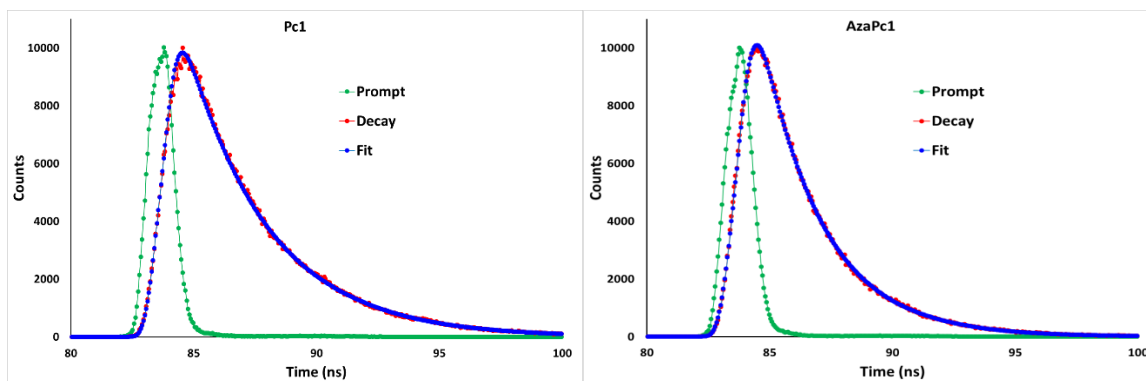


**Figure S34.** Time correlated single photon counting (TCSPC) fluorescence decay curve of **Pc1/AzaPc1** in DMF.

## Singlet oxygen quantum yields

Transferring of energy from the triplet state of a photosensitizer such as Pc to ground state molecular oxygen leads to the production of singlet oxygen. There is a necessity of high efficiency of energy transfer between the excited triplet state of photosensitizer and the ground state of oxygen in order to generate large amounts of singlet oxygen, essential for PDT applications. The singlet oxygen quantum yield ( $\Phi_{\Delta}$ ) values give the amount of the generated singlet oxygen. This value is an indication of the potential provided by the compounds as photosensitizers in applications where singlet oxygen is required. The  $\Phi_{\Delta}$  values for **Pc1/AzaPc1** were determined in DMF by a chemical method using 1,3-diphenylisobenzofuran (DPBF) as a quencher. The disappearance of DPBF at 414 nm was monitored using UV-Vis spectrophotometer. Many factors can be responsible for the magnitude of the determined singlet oxygen quantum yield including such as triplet excited state energy, ability of substituents and solvents to quench the singlet oxygen, the triplet excited state lifetime and the efficiency of the energy transfer between the triplet excited state and the ground state of oxygen. Any changing did not observe in the Q band intensities of all cyclic complexes suggesting that all **Pc1/AzaPc1** did not show any decomposition during singlet oxygen studies (Figure S35). Both macrocyclic derivatives showed similar singlet oxygen generation with  $\Phi_{\Delta}$  around 0.6. Both cyclic structures are suggested suitable candidates as photosensitizers for cancer treatment by photodynamic therapy method due to their high singlet oxygen production abilities.

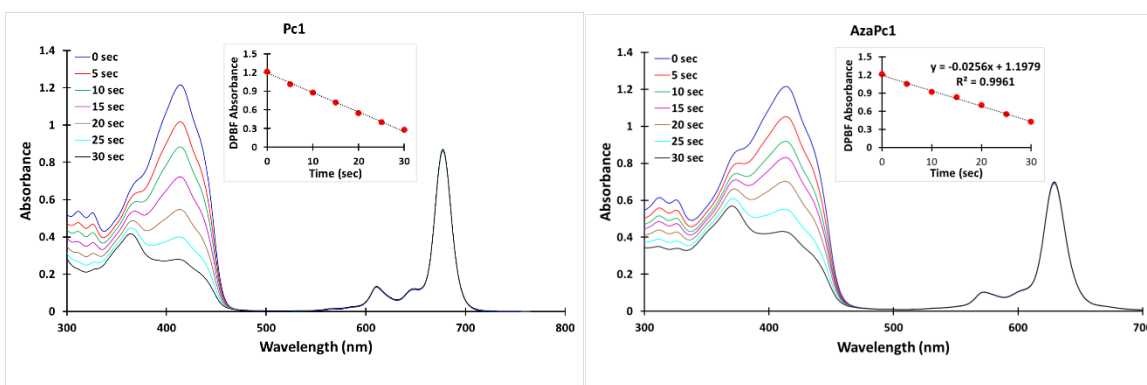


**Figure S35.** Absorbance changes during the determination of singlet oxygen quantum yield of **Pc1/AzaPc1** in DMF. (Inset: Plot of DPBF absorbances versus irradiation time).

## Photodegradation quantum yields

Photodegradation is used to specify the stability of compounds which is useful for determination of the photosensitizing ability of the compounds as PDT agents. The stability of photosensitizers under light irradiation is important for photochemical processes such as PDT because photosensitizers need to survive for a specific period in the body. Photodegradation degree can be detected by photodegradation quantum yield ( $\Phi_d$ ) and it depends on the structure, light intensity, used solvent and the concentration.<sup>[4]</sup> Photodegradation of the compounds under light irradiation can be used to study their stability which is important for those molecules intended for the application in photocatalytic reactions. The collapse of the absorption spectra without any distortion of the shape confirms photodegradation not associated with phototransformation into different forms of Pcs absorbing light in the visible region. The spectral changes for all macrocyclic derivatives during light irradiation are confirmed photodegradation occurred without photo transformation because only Q and B bands were decreased, and no new band formation was observed (Figure S36). Pc and their macrocyclic analogs generate singlet oxygen when they are illuminated by an appropriate light. The formed singlet oxygen is partially degraded by the Pc/Pc-analogs *via* photooxidation reactions. Generally, photodegradation of the Pcs/Pc-analogy compounds by light irradiation results in formation of the phthalamide residue. The photodegradation behavior of **Pc1** and **AzaPc1** were determined in DMF. The  $\Phi_d$  values of these novel systems were found the order of  $10^{-4}$  (Table S1) and these values are similar with those Pcs containing different metals and substituents.<sup>[13]</sup>

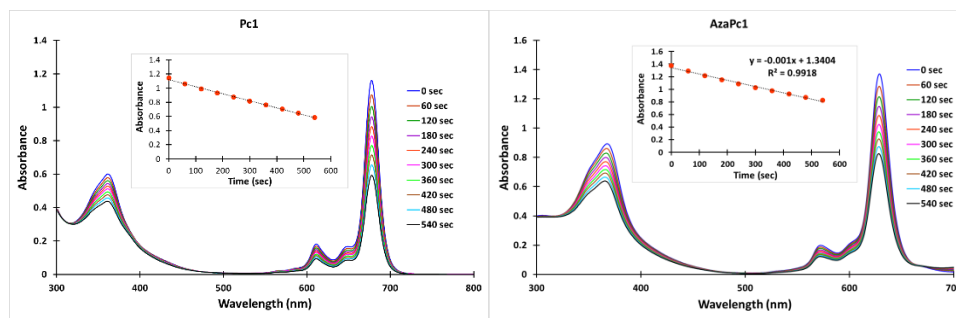


**Figure S36.** Absorbance changes during the photodegradation study of **Pc1/AzaPc1** in DMF showing the decreasing of the absorption bands at 60 sec intervals (Inset: Plot of Q band absorbance versus irradiation time).

## Excited triplet state

The triplet-state life time ( $\tau_T$ ), the quantum yield ( $\Phi_T$ ) and the molar absorption coefficient ( $\Delta\epsilon_T$ ) were calculated for both of the studied complexes (Table S2). The  $\tau_T$  values were calculated to be 1231  $\mu\text{s}$  for **Pc1** and 400  $\mu\text{s}$  for **AzaPc1**, which are longer than the lifetimes previously reported for standard ZnPc, and these values are long enough to allow the production of singlet oxygen. This very long triplet lifetime could be attributed to the obstruction of solvent collision by the multiple bulky phenoxy units on the periphery. These large substituents in **Pc1** result in higher structural rigidity and thus offer more protection, which makes the  $\tau_T$  of **Pc1** larger. On the other hand, in air-saturated solutions, the measured  $\tau_T$  values for both complexes decreased dramatically to 1.2 $\mu\text{s}$  for **Pc1** and to 1.9 $\mu\text{s}$  for **AzaPc1** compared to 0.30  $\mu\text{s}$  of ZnPc, and their TAS spectra did not change noticeably, i.e., the shape and spectral position remained constant, confirming the effective quenching of molecular oxygen by a physical process ( $T_1 + O_2 \rightarrow S_0 + {}^1O_2$ ), and consequently, the positive absorptions can confidently be attributed to  $T_1$ - $T_n$  triplet absorptions (Figure S37). The formation of the triplet species ( $\Phi_T$ ) by each of the two complexes was evaluated, and they were found to be very close to their  $\Phi_\Delta$  values, as shown in Table S2, suggesting an effective interaction between their triplet states and the molecular oxygen present in the system, resulting in a high quantum yield of singlet oxygen (% of  $\Phi_\Delta/\Phi_T \approx 96$  for **Pc1** and 98 for **AzaPc1**). However, the total yields of both fluorescence and the triplet state of the two macrocycles are comparable and are less than one, indicating the presence of internal conversion ( $\Phi_{IC} = 1 - \Phi_F - \Phi_T$ ). The LFP confirms the formation of T with a very high quantum yield and a long life time from the studied complexes, which make them an important class of compounds for many applications.

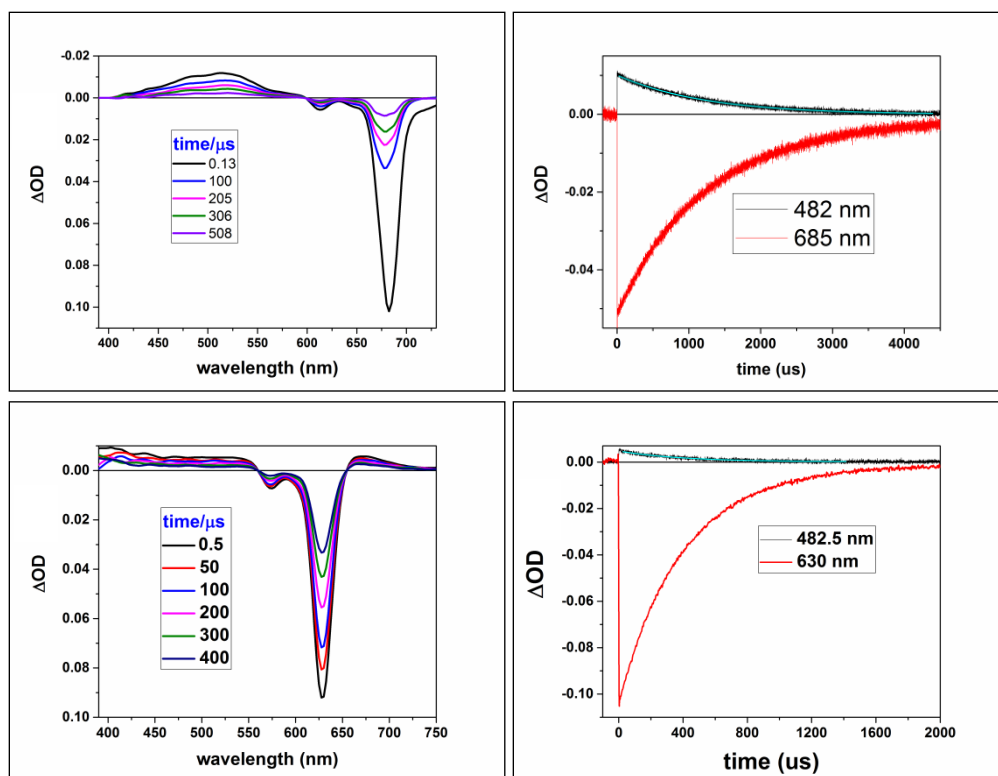


**Figure S37. Left:** time resolved  $T_1$ - $T_n$  transient absorption spectra of 20  $\mu M$  compound **Pc1**(top) and **AzaPc1** (bottom) in nitrogen saturated DMF with OPO laser excitation (4 ns, 5 mJ) at 686 and 637 nm, respectively. **Right:** The decay of  $T_1$  state and the concomitant rise of ground state for 20  $\mu M$  compound **Pc1**(top) and **AzaPc1** (bottom) in nitrogen saturated DMF with OPO laser excitation (4 ns, 5 mJ).

**Table S1.** Electronic absorption and steady state properties of **Pc1**, **Pc2**, **AzaPc1** and **AzaPc2** in DMF.<sup>[a]</sup>

Comp.	Log $\epsilon$	$\lambda_{\text{abs}}(\text{nm})$	$\lambda_{\text{ex}}(\text{nm})$	$\lambda_{\text{em}}(\text{nm})$	$\Delta\lambda(\text{nm})$	$\Phi_{\text{F}}$	$\tau_{\text{F}}(\text{ns})$	$K_{\text{f}}(\text{s}^{-1})$ ( $\times 10^9$ )	$K_{\text{nr}}(\text{s}^{-1})$ ( $\times 10^9$ )	$\Phi_{\text{d}}(10^{-4})$
<b>Pc1</b>	5.33	678	679	683	4	0.16	3.30	0.048	0.254	1.58
<b>AzaPc1</b>	5.07	629	629	639	10	0.14	2.46	0.056	0.349	4.30
<b>Pc2</b>	5.37	681	682	690	8	0.10	2.90	0.203	0.321	0.30
<b>AzaPc2</b>	5.15	631	631	638	7	0.10	2.45	0.039	0.369	7.40
<b>StdZnPc<sup>b</sup></b>	5.37	670	670	676	6	0.17	1.03	0.165	0.805	0.23

<sup>[a]</sup> $\epsilon$ : Excitation coefficient,  $\lambda_{\text{abs}}$ ; Q-band absorption maximum wavelength,  $\lambda_{\text{ex}}$ ; Excitation maximum wavelength,  $\lambda_{\text{em}}$ ; Emission maximum wavelength,  $\Delta\lambda$ ; Stokes shift,  $\Phi_{\text{F}}$ ; Fluorescence quantum yield,  $\tau_{\text{F}}$ ; Fluorescence lifetime,  $K_{\text{f}}$ ; Rate constant of emission process ( $\kappa_{\text{f}} = \Phi_{\text{F}}/\tau_{\text{F}}$ ),  $K_{\text{nr}}$ ; Non-radiative rate constants ( $K_{\text{nr}} = ((1-\Phi_{\text{F}}))/\tau_{\text{F}}$ ),  $\Phi_{\text{d}}$ ; Photodegradation quantum yield.

<sup>[b]</sup>**Std-ZnPc**; was used as a reference compound.<sup>[3, 6, 14]</sup>

**Table S2.** Excited triplet state properties and singlet oxygen formation yield in DMF.<sup>[a]</sup>

Comp.	$\Phi_{\Delta}$	$\Delta\text{s}$	$\Phi_{\text{T}}$	$\lambda_{\text{T-T}}(\text{nm})$	$\Delta \epsilon_{\text{T-T}}(\text{m}^{-1} \text{cm}^{-1})$	$\tau_{\text{T}}(\mu\text{s})/\text{N}_2$	$\tau_{\text{T}}(\mu\text{s})/\text{air}$	$K_{\text{q}}(10^{-9}\text{M}^{-1} \text{S}^{-1})$
<b>Pc-1</b>	0.60	0.97	0.62	513	34115	1231	1.2	0.42
<b>AzaPc1</b>	0.63	0.98	0.64	410	17175	400	1.9	0.26
<b>Std-ZnPc<sup>[b]</sup></b>	0.56 <sup>c</sup>	1.00	0.56	480	33300 <sup>26</sup>	330	0.30	1.66

<sup>[a]</sup>  $\Phi_{\Delta}$ ; singlet oxygen quantum yield,  $\Delta\text{s}$ ; fraction triplet state deactivated by oxygen,  $\Phi_{\text{T}}$ ; triplet state quantum yield,  $\lambda_{\text{T-T}}$ ; triplet-triplet absorption maximum,  $\Delta\epsilon_{\text{T-T}}$ ; triplet-triplet coefficient,  $\tau_{\text{T}}$ ; triplet state lifetime,  $K_{\text{q}}$ ; triplet quenching rate constant by oxygen.

<sup>[b]</sup>**StdZnPc** was used as a reference compound.<sup>[3, 6, 14]</sup>

## Single crystal X-ray diffraction studies of propargyl functionalized phthalocyanine analogues and their precursors

### Experimental

The single crystal data collections were made either on Rigaku R-AXIS RAPID II diffractometer by filtered Mo-K $\alpha$  radiation or using Bruker X8 Prospector employing Cu-K $\alpha$  radiation. In the former case ‘Crystalclear’ software package was employed to generate hkl and p4p files. The structures were then solved by direct methods using CrystalStructure crystallographic software package<sup>[15]</sup> except for refinement, which was performed using SHELXL-97 or SHELXL-2017/1.<sup>[16]</sup> The reflection frames obtained from Bruker diffractometer were integrated with SAINT Software package using a narrow-frame algorithm. Finally, the structure was solved and refined using the Bruker SHELXTL Software Package. The data was collected either at room temperature or under liquid nitrogen (Oxford cryosystems).

### Discussion

#### Crystal structures of di-propargyl-*p*-cresol (2)

The structure of propargyl functionalized *p*-cresol is confirmed further by single crystal X-ray diffraction technique which is depicted in Figure S38. The crystal structure is in well agreement with other (NMR, mass etc.) structural characterization. It is observed that in crystal network the propargyl substituents are oriented opposite to each other and are placed above and below the cresol plane as shown in Figure S38B.

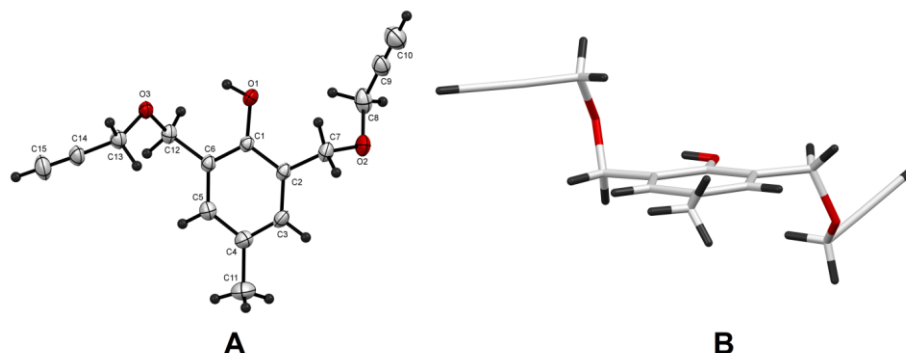


**Figure S38.** Crystal structure propargyl functionalized *p*-cresol; (A) thermal ellipsoid and (B) capped stick representation.

### Crystal structures of propargyl substituted Pc-precursor (3) and AzaPc-precursors (4)

Phthalonitrile and pyrazine precursors having both di-substituted phenoxy groups with terminal acetylene units were analyzed by single crystal X-ray diffraction technique. The crystal structure of both these precursors provides valuable information regarding the orientation of phenoxy units and terminal acetylenes with respect to the phthalonitrile/pyrazine planes. The structures of phthalonitrile and pyrazine substrates with propargyl moieties, which are obtained from single crystal diffraction analysis, are depicted in Figures S39 & S40 and their corresponding crystallographic parameters are given in Table S3. The plane of the phenoxy ring having the terminal alkynyl groups are oriented almost perpendicular to the plane of the phenyl rings containing the nitrile groups (the corresponding torsion angles are presented in Table S4. This is due to the restricted rotation imposed on phenoxy moieties by the bulky alkyne substituents which are presented at the ortho positions of the phenyl groups. Such a blocked rotation caused by the propargyl chains is sufficient for ensuring the non-aggregating feature for those Pc systems which will be synthesized from these unique molecules by the metal mediated cyclization. The terminal propargyl groups have sufficient chain length for flexible orientations are projected randomly in their crystal network. Their packing is very efficient so that without having any solvent co-crystallization, these crystals are stable enough for diffraction studies.

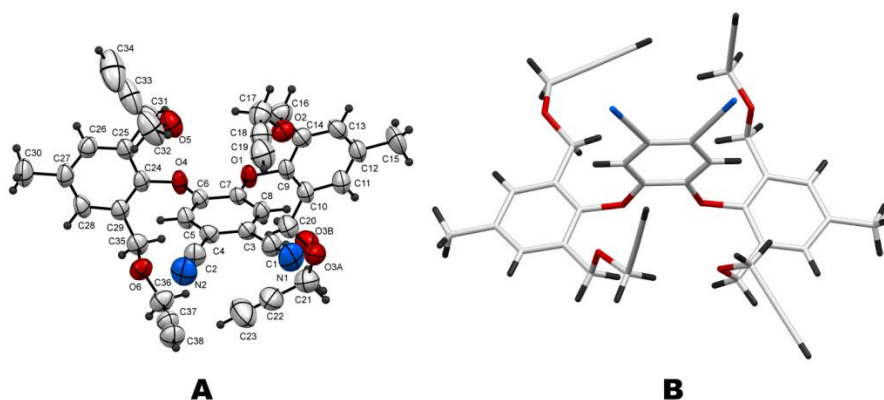


**Figure S39.** Crystal structure of **3** obtained from diffraction data (**A**)-thermal ellipsoid representation and (**B**)-capped stick representation. Color code: blue-nitrogen; gray-carbon; red oxygen; and black-hydrogen.

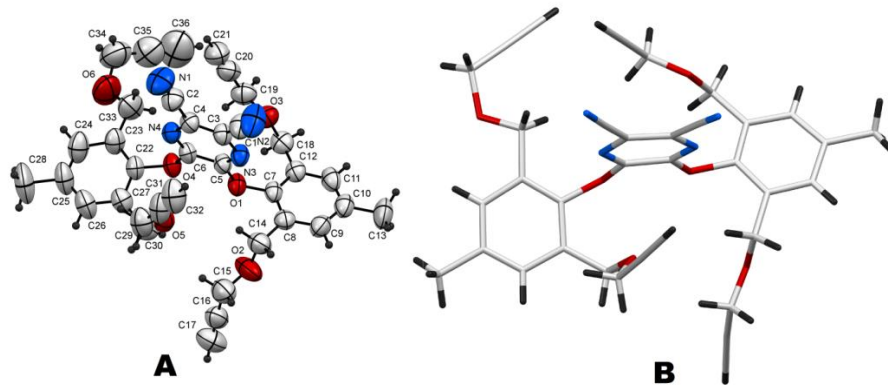


**Figure S40.** Crystal structure of **4** obtained from diffraction data (**A**)-thermal ellipsoid representation and (**B**)-capped stick representation. Color code: blue-nitrogen; gray-carbon; red oxygen; and black-hydrogen.

**Table S3.** Summary on the nature and various crystallographic parameters of crystal samples of precursors **3** and **4**.

Crystal sample	<b>3</b>	<b>4</b>
<b>Crystal data</b>		
Chemical formula	C <sub>38</sub> H <sub>32</sub> N <sub>2</sub> O <sub>6</sub>	C <sub>36</sub> H <sub>30</sub> N <sub>4</sub> O <sub>6</sub>
<i>M<sub>r</sub></i>	612.65	614.64
Crystal system, space group	Monoclinic, <i>P2<sub>1</sub>/n</i>	Monoclinic, <i>P2<sub>1</sub>/n</i>
Temperature (K)	296	296
<i>a</i> , <i>b</i> , <i>c</i> (Å)	12.6219 (11), 16.3765 (13), 16.6547 (14)	12.8709 (4), 15.6947 (4), 16.5272 (5)
β (°)	100.607 (4)	92.507 (2)
<i>V</i> (Å <sup>3</sup> )	3383.7 (5)	3335.38 (17)
<i>Z</i>	4	4
Radiation type	Cu <i>K</i> α	Cu <i>K</i> α
μ (mm <sup>-1</sup> )	0.66	0.69
Crystal size (mm)	0.22 × 0.11 × 0.05	0.30 × 0.20 × 0.07
<b>Data collection</b>		
Diffractometer	Bruker X8 Prospector	Bruker X8 Prospector
Absorption correction	Multi-scan	Multi-scan
	<i>SADABS</i> V2008/1 (Bruker)	<i>SADABS</i> V2008/1 (Bruker)
<i>T<sub>min</sub></i> , <i>T<sub>max</sub></i>	0.60, 0.87	0.70, 0.96
No. of measured, independent and observed [ <i>I</i> > 2σ( <i>I</i> )] reflections	23446, 5674, 4020	28049, 5828, 2669
<i>R<sub>int</sub></i>	0.058	0.154
(sin θ/λ) <sub>max</sub> (Å <sup>-1</sup> )	0.593	0.595
<b>Refinement</b>		
<i>R</i> [ <i>F</i> <sup>2</sup> > 2σ( <i>F</i> <sup>2</sup> )], w <i>R</i> ( <i>F</i> <sup>2</sup> ), <i>S</i>	0.083, 0.207, 1.13	0.071, 0.260, 1.00
No. of reflections	5674	5828
No. of parameters	427	417
No. of restraints	54	31
H-atom treatment	Constrained	Constrained
Δρ <sub>max</sub> , Δρ <sub>min</sub> (e Å <sup>-3</sup> )	0.24, -0.28	0.44, -0.26

**Table S4.** List of torsion angles corresponds to the phenoxy with respect to the di-nitrile plane in **3** and **4**.

Atom list	Torsion angle	Atom list	Torsion angle
<b>Crystal: 3</b>			
C10-C9-O1-C7	C10-C9-O1-C7	C10-C9-O1-C7	C10-C9-O1-C7
C25-C24-O4-C6	C25-C24-O4-C6	C25-C24-O4-C6	C25-C24-O4-C6
<b>Crystal: 4</b>			
C8-C7-O1-C5	C8-C7-O1-C5	C8-C7-O1-C5	C8-C7-O1-C5
C23-C22-O4-C6	C23-C22-O4-C6	C23-C22-O4-C6	C23-C22-O4-C6

### Crystal structures of **Pc1** and **AzaPc1**

The crystal structures of **Pc1** and **AzaPc1** are depicted in Figures S41-44 and their corresponding crystallographic parameters are presented in Table S5. The asymmetric unit of **Pc1** crystal contains only half part of the phthalocyanine due to internal symmetry of the molecule and the complete structure could be obtained by symmetry expansion. In both **Pc1** and **AzaPc1** the zinc (II) ion occupied at the top of the Pc/AzaPc plane and the phthalocyanine/azaphthalocyanine macrocycles is observed to have a domed geometry. The **Pc1** molecule in crystal network exhibited positional disorder at the center and due to this disorder, the Zn (II) ion in **Pc1** crystal is found to be occupied both sides of the Pc plane with almost half occupancies each. In the case of **AzaPc1**, one methanol molecules is coordinated from the apex position to the Zn (II) ion, where as in **Pc1** such axial ligation of solvent molecule is not observed. However, two terminal alkynyl groups are occupied very close to the Zinc (II) ion of the **Pc1** so that appreciable Zn ← C ≡ C-H coordination could be possible in its crystal. Due to positional disorder, this Zn ← C ≡ C-H coordination is observed from both sides of the Pc unit and hence is seen to be propagate along the crystal in columnar manner as demonstrated in Figure S45.

The crystal network of **AzaPc1** contains methanol molecules as the space-filling solvents which are co-crystallized along with the AzaPc molecules during crystal growth. The peak densities of these solvent molecules were very weak and they are not properly refined anisotropically during structural refinement. So these solvent molecules in **AzaPc1** are only refined isotropically. In the case of **AzaPc1** some electron density is present within the void places by the presence of co-crystallized solvent molecules. Due to poor crystal quality these peaks could not be assigned to

the corresponding solvent atoms properly. Therefore, these unassigned solvent peaks were removed from the final refinement using the SQUEEZE technique by PLATON.

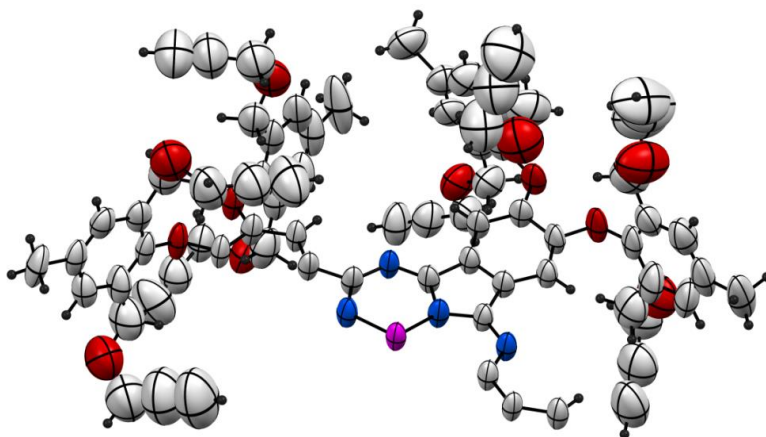


**Figure S41.** Thermal ellipsoid representation of the asymmetric unit of **Pc1** obtained from single crystal diffraction. Color code: blue-nitrogen; gray-carbon; red-oxygen; pink- zinc and black-hydrogen.

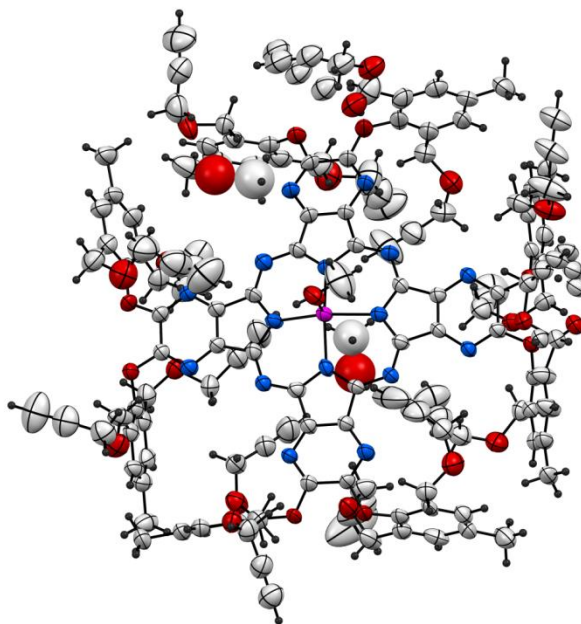


**Figure S42.** Thermal ellipsoid representation of **AzaPc1** obtained from single crystal diffraction. Color code: blue-nitrogen; gray-carbon; red-oxygen; pink- zinc and black-hydrogen.

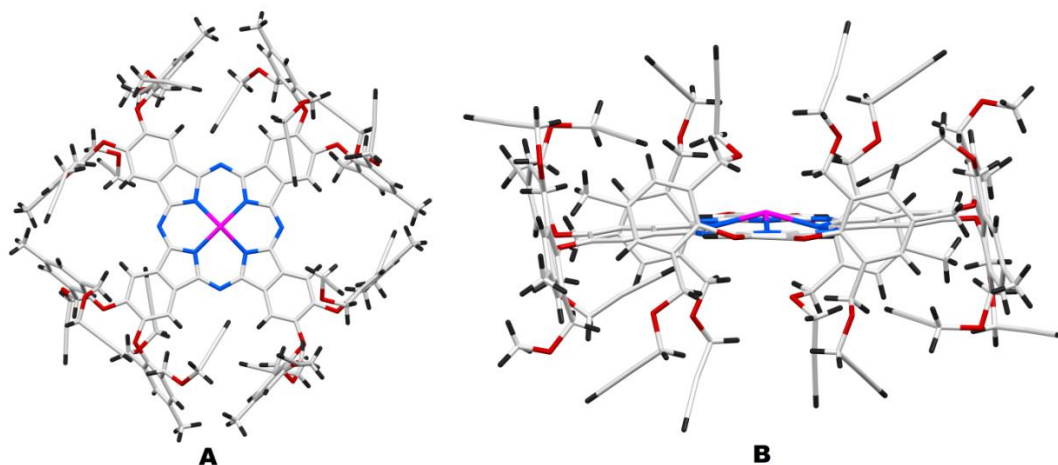


**Figure S43.** Crystal structure of **Pc1**(**A**) top view and (**B**) side view. Color code: blue-nitrogen; gray-carbon; red-oxygen; pink- zinc and black-hydrogen (due to positional disorder, the Zn ion in this crystal is found to be occupied at both sides of the Pc plane with half occupancies. However, one of such Zn ions has been hid in these figures for clarity).

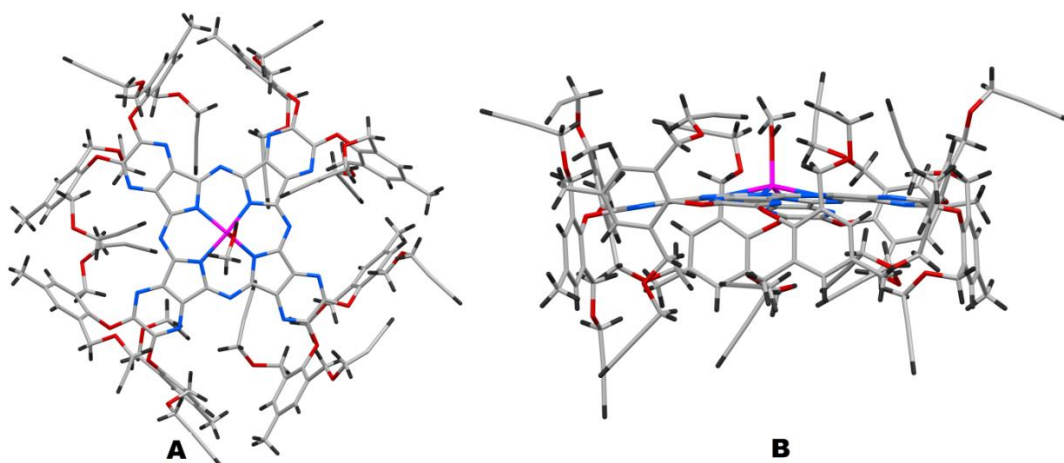


**Figure S44.** Crystal structure of **AzaPc1**(**A**) top view and (**B**) side view. Color code: blue-nitrogen; gray-carbon; red-oxygen; pink- zinc and black-hydrogen.

**Table S5.** Summary on the nature and various crystallographic parameters of crystal samples **Pc1** and **AzaPc1**.

Crystal sample	AzaPc1	Pc1
<b>Crystal data</b>		
Chemical formula	C <sub>147</sub> H <sub>132</sub> N <sub>16</sub> O <sub>27</sub> Zn	C <sub>152</sub> H <sub>128</sub> N <sub>8</sub> O <sub>24</sub> Zn
$M_r$	2620.06	2515.99
Crystal system, space group	Monoclinic, $P2_1/a$	Triclinic, $P-1$
Temperature (K)	150	150
$a, b, c$ (Å)	23.940 (11), 28.050 (13), 23.991 (11)	12.8844 (13), 13.9073 (13), 20.6328 (19)
$\alpha, \beta, \gamma$ (°)	119.850 (8)	98.862 (7), 106.525 (7), 94.899 (7)
$V$ (Å <sup>3</sup> )	13973 (11)	3469.4 (6)
$Z$	4	1
Radiation type	Mo $K\alpha$	Mo $K\alpha$
$\mu$ (mm <sup>-1</sup> )	0.25	0.25
Crystal size (mm)	0.22 × 0.19 × 0.03	0.21 × 0.12 × 0.09
<b>Data collection</b>		
Diffractometer	Rigaku R-AXIS RAPID	Rigaku R-AXIS RAPID
Absorption correction	Multi-scan	Multi-scan
	ABSCOR (Rigaku, 1995)	ABSCOR (Rigaku, 1995)
$T_{\min}, T_{\max}$	0.947, 0.993	0.950, 0.978
No. of measured, independent and observed [ $I > 2\sigma(I)$ ] reflections	102734, 24158, 14696	27487, 12186, 6351
$R_{\text{int}}$	0.081	0.032
$(\sin \theta/\lambda)_{\text{max}}$ (Å <sup>-1</sup> )	0.596	0.595
<b>Refinement</b>		
$R[F^2 > 2\sigma(F^2)], wR(F^2), S$	0.129, 0.365, 1.26	0.138, 0.420, 1.45
No. of parameters	1798	842
No. of restraints	431	241
H-atom treatment	Independent and constrained	Constrained
$\Delta\rho_{\text{max}}, \Delta\rho_{\text{min}}$ (e Å <sup>-3</sup> )	2.86, -0.77	1.17, -0.76

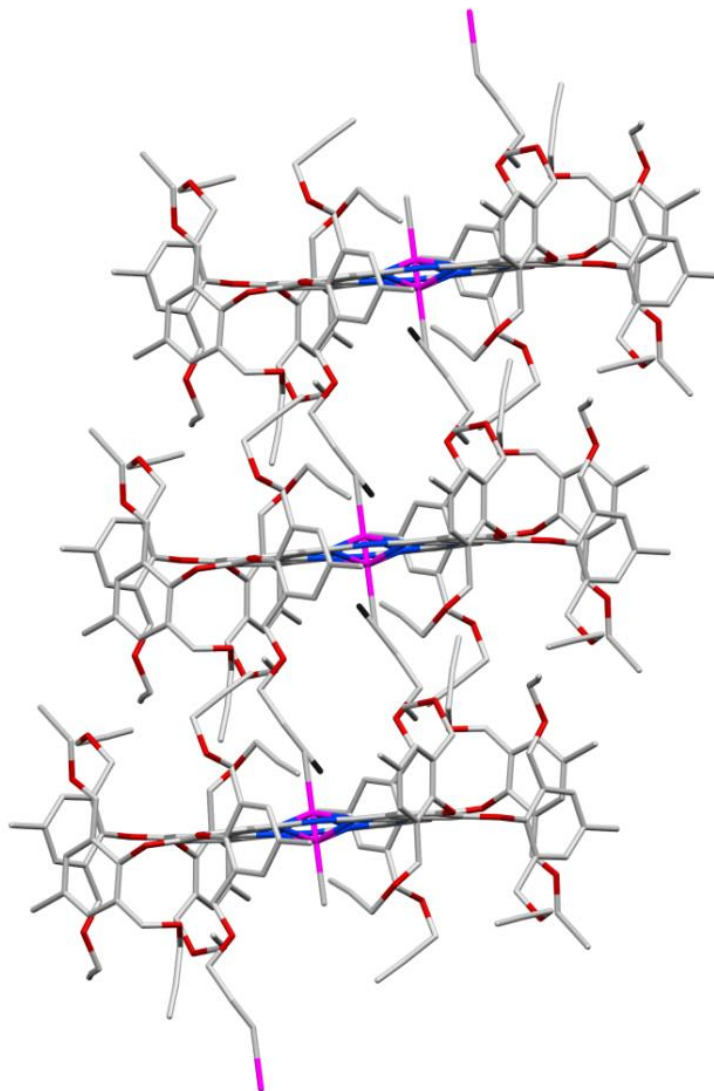


**Figure S45.** The Zn ← C ≡ C-H coordination observed from both sides of the Pc unit and the resulting columnar propagation of the macrocycles.

As in the case of their pyrazine and phthalonitrile precursors, the phenoxy units containing the propargyl units are oriented orthogonal with respect to the plane of Pc ring. These terminal alkynes which are presented at the ortho positions of the phenoxy moieties are mostly oriented upward and downward from the macrocycle planes in a random arrangement. Figures S43 and S44, which show both top view and side view of these crystal structures, provides a clear idea about the terminal ethylene orientations with respect to macrocycle planes. Such an orthogonal orientation of the phenoxy units and the resulting positions of the terminal propargyl moieties

(up/down) with respect to the macrocycle planes as revealed from the crystal structures clearly dismiss any possible face to face Pc aggregation among these Pc molecules. In both these crystals the Zn-Zn distance is more than  $10\text{\AA}$  which is too far to cause the undesired J-type core to core Pc self-aggregation. However, unlike their precursor molecules, the special disposition of propargyl groups in **Pc1** and **AzaPc1** crystals are not exactly similar as the terminal alkynes are more widely oriented in **Pc1** than **AzaPc1**. This difference could be presumably due to the difference in axial coordination, variations in crystallization conditions, etc.

The packing of both **Pc1** and **AzaPc1** molecules in their crystal is very and efficient by utilizing intermolecular  $\pi$ - $\pi$  interactions with adjacent Pcs. As demonstrated in Figure S46, all phenoxy moieties in these crystals are oriented in face- to face manner with another phenoxy unit of neighboring Pcs. It is observed that the distance between such phenoxy-phenoxyl face to face orientations is within  $4\text{\AA}$  in most fragments which is well sufficient for intermolecular  $\pi$ - $\pi$  interactions. Such 2-dimensional  $\pi$ - $\pi$  interactions between adjacent phenoxy moieties provide sufficient stability to these crystal samples.

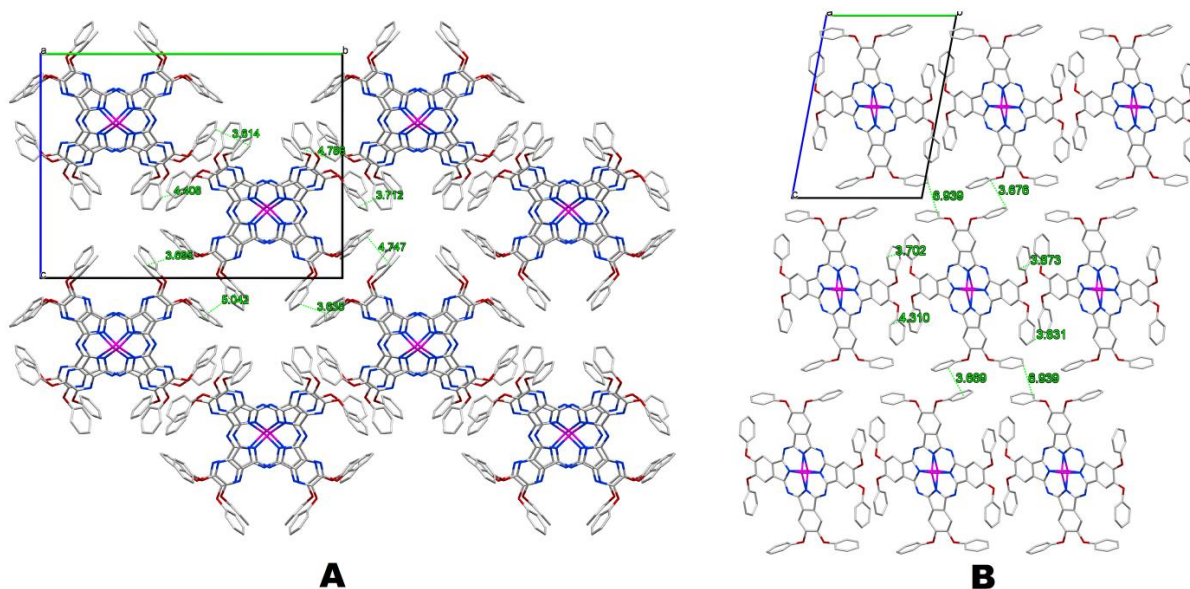


**Figure S46.** Pattern of **Pc1** and **AzaPc1** molecules in their crystal network showing the intermolecular  $\pi$ - $\pi$  interactions through phenoxy moieties; (A) **AzaPc1** and (B) **Pc1**. The terminal substituents and hydrogens are hidden for clarity.

The unit cells of these phthalocyanine crystals are depicted in Figure S47 and the packing sequence in Figure S48 (where the peripheral substituents are hid for clarity). In the case of AzaPc, the arrangements of **AzaPc1** molecules are in such a way that along a- and c-direction all molecules in each row are arranged in the same manner and direction, whereas along b- direction are arranged in zig-zag manner with adjacent AzaPcs are inverted to each other (Figures S48 and S49). This is much clearly demonstrated in Figure S50 which shows the arrangements of AzaPc core structure where all peripheral substituents are hid for clarity. At the same time, in the case of **Pc1** crystals, Pc molecules in each row along all 3 directions namely a-, b-, c-, are oriented in same way as demonstrated in Figures S51 and S52.

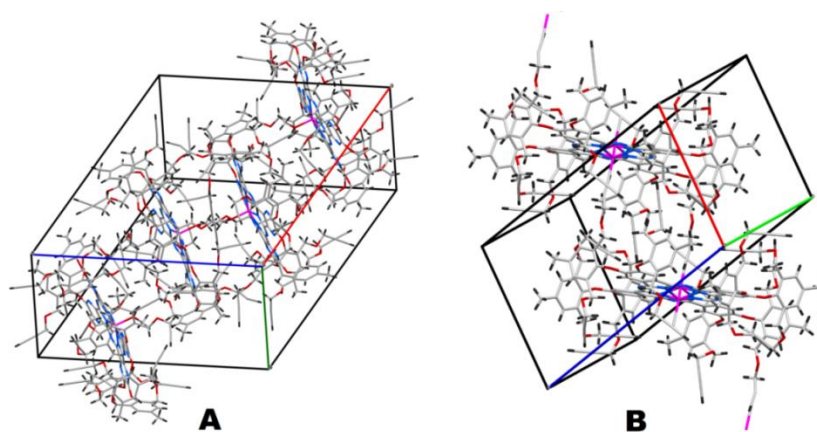


**Figure S47.** The unit cell of (A) **AzaPc1** and (B) **Pc1** crystals. Color code: red-oxygen; blue-nitrogen; pink- Zinc; gray-carbon and black-hydrogen.

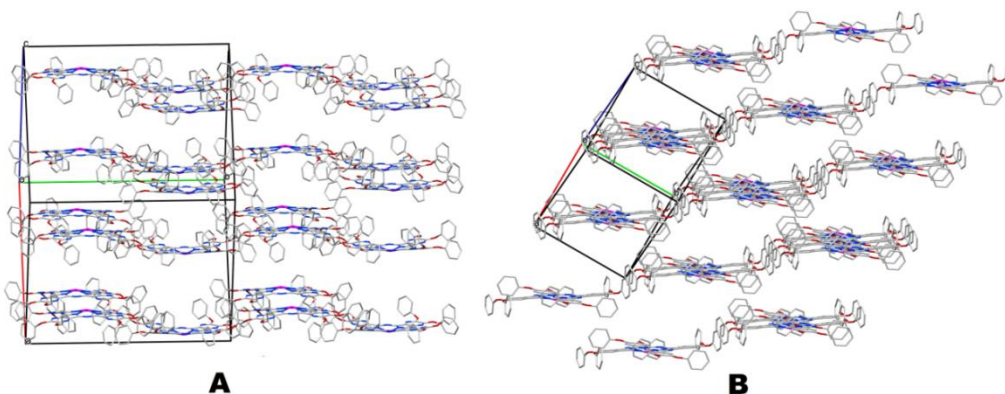


**Figure S48.** The packing of (A) **AzaPc1** and (B) **Pc1** molecules in their crystals. The terminal substituents and hydrogen atoms are hid for clarity

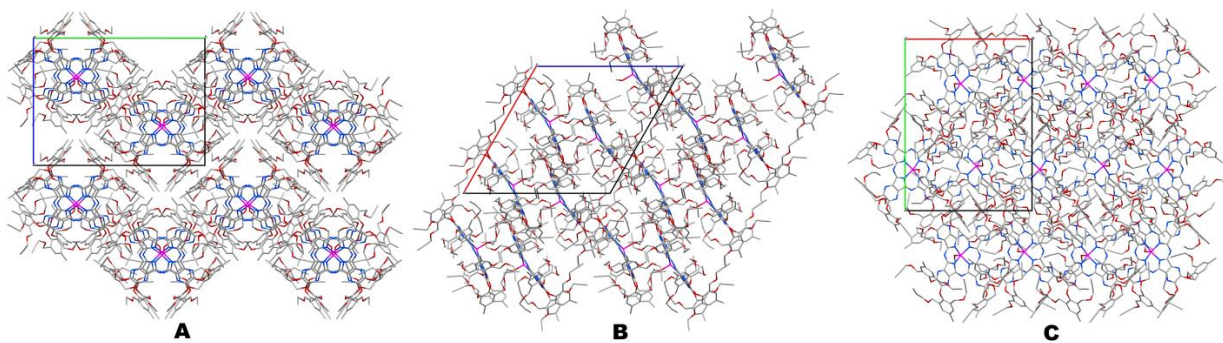


**Figure S49.** Packing pattern of **AzaPc1** in their crystal network; **A**- view along the a-direction; **B**- along the b-direction and **C**- along the c-direction. Color code: red-oxygen; blue-nitrogen; gray-carbon; and pink- zinc (hydrogens and solvents has been hided for clarity).

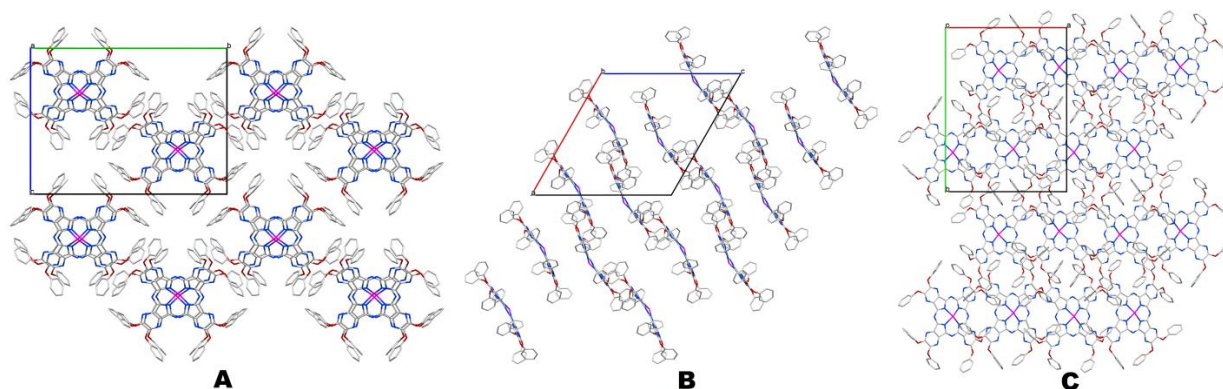


**Figure S50.** Packing pattern of **Pc1** in their crystal network; **A**- view along the a-direction; **B**- along the b-direction and **C**- along the c-direction. The terminal substituents, solvents and hydrogens are hided for clarity.

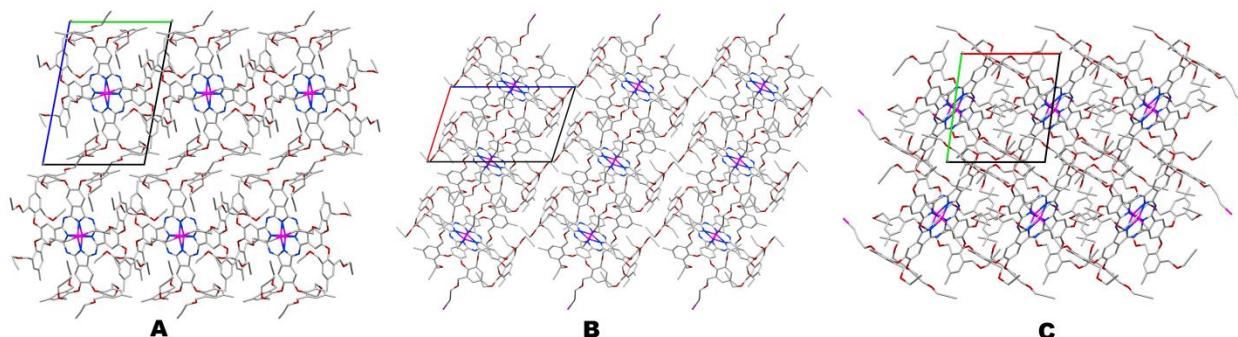


**Figure S51.** Packing pattern of **Pc1** in their crystal network; **A**- view along the a-direction; **B**- along the b-direction and **C**- along the c-direction. Color code: red-oxygen; blue-nitrogen; gray-carbon; and pink- zinc (hydrogens has been hided for clarity).

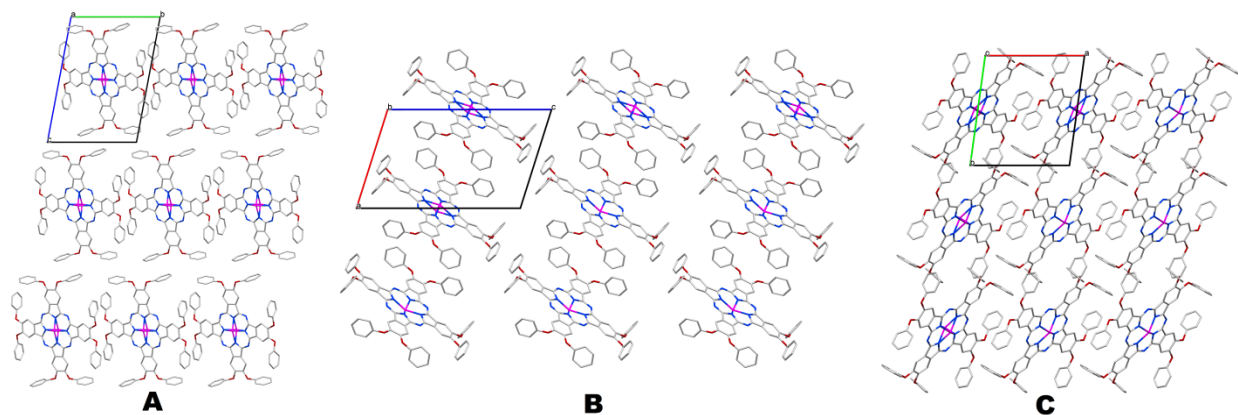


**Figure S52.** Packing pattern of **Pc1** in their crystal network; **A**- view along the a-direction; **B**- along the b-direction and **C**- along the c-direction. The terminal substituents and hydrogen atoms are hidden for clarity.

In addition to the efficient 2-dimensional  $\pi$ - $\pi$  interactions between adjacent phenoxy moieties among the **Pc1** and **AzaPc1** molecules, the crystals are also stabilized by van der waals interactions between adjacent atoms. The possible short contact interactions (within the van der waals range) observed in these crystals are depicted in Figure S53.

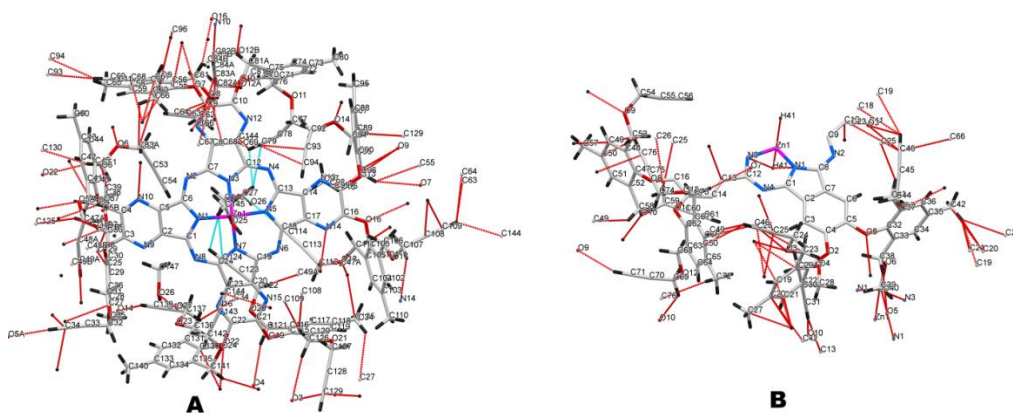


**Figure S53.** The molecules of (A) **AzaPc1** and (B) **Pc1** in their crystals showing their possible short contacts interactions among the neighboring atoms within their network.

In conclusion, the crystal structures of hexadeca-propargyl functionalized zinc(II) phthalocyanine (**Pc1**) and their corresponding azaphthalocyanine analogue (**AzaPc1**) have been obtained from single crystal X-ray diffraction technique along with the structures of some

phthalonitrile and pyrazine precursor units having terminal propargyl moieties (**3** and **4**). Based on the crystal structure it could be confirmed that for all these precursors, plane of the phenoxy ring having terminal alkyne groups are oriented perpendicular to the plane of the phenyl moiety containing the nitrile groups. This is due to the restricted rotation imposed on phenoxy moieties by the bulky alkynyl substituents which are presented at the ortho positions of the phenyl groups. This orthogonal orientation is observed in both precursor species irrespective of the number of phenoxy substitution. In both **Pc1** and **AzaPc1**, the macrocycle systems are observed to have a domed geometry with zinc (II) ion occupied at the top of the Pc/AzaPc plane. Similar to the case of their precursors, the phenoxy units containing the propargyl units are oriented orthogonal with respect to the plane of Pc/AzaPc ring in both **Pc1** and **AzaPc1** and the terminal alkynes moieties are oriented upward and downward from the Pc rim in a random arrangement. Such an orthogonal orientation of the phenoxy units and the resulting positions of the terminal propargyl moieties (up/down) with respect to the Pc plane dismiss undesired face to face Pc/AzaPc aggregation among these Pc/AzaPc molecules. At the same time, these crystals are characterized by high degree of 2-dimensional  $\pi$ - $\pi$  interactions between adjacent phenoxy moieties of Pc/AzaPc macrocycles which provide sufficient stability to these crystal samples.

## References

- [1] W. L. F. Armarego, D. D. Perrin, Butterworth Heinemann, Oxford; Boston, **1997**.
- [2] a) S. Fery-Forgues, D. Lavabre, *Journal of Chemical Education* **1999**, 76, 1260; b) M. D. Maree, T. Nyokong, K. Suhling, D. Phillips, *Journal of Porphyrins and Phthalocyanines* **2002**, 06, 373-376.
- [3] Y. Zorlu, F. Dumoulin, M. Durmuş, V. Ahsen, *Tetrahedron* **2010**, 66, 3248-3258.
- [4] M. Durmuş, *Photochemical and Photophysical Characterization*, Springer Dordrecht Heidelberg London New York, **2012**.
- [5] W. Spiller, H. Kliesch, D. Wöhrle, S. Hackbarth, B. Röder, G. Schnurpfeil, *Journal of Porphyrins and Phthalocyanines* **1998**, 2, 145-158.
- [6] I. Carmichael, G. L. Hug, *Journal of Physical and Chemical Reference Data* **1986**, 15, 1-250.
- [7] S. M. Bishop, A. Beeby, A. W. Parker, M. S. C. Foley, D. Phillips, *Journal of Photochemistry and Photobiology A: Chemistry* **1995**, 90, 39-44.
- [8] B. M. Trost, V. S. C. Yeh, H. Ito, N. Bremeyer, *Organic Letters* **2002**, 4, 2621-2623.
- [9] N. T. Stillman MJ, in: Leznoff CC, Lever ABP *Phthalocyanines, Properties and Applications, Vol. 1*, VCH Publishers, **1989**.
- [10] a) H. Konami, M. Hatano, A. Tajiri, *Chemical Physics Letters* **1990**, 166, 605-608; b) J. Mack, M. J. Stillman, *Journal of the American Chemical Society* **1994**, 116, 1292-1304.
- [11] H. ENGELKAMP, R. J. M. NOLTE, *Journal of Porphyrins and Phthalocyanines* **2000**, 04, 454-459.
- [12] T. Nyokong, *Coordination Chemistry Reviews* **2007**, 251, 1707-1722.
- [13] M. Göksel, M. Durmuş, D. Atilla, *Journal of Porphyrins and Phthalocyanines* **2012**, 16, 895-906.
- [14] a) M. Durmuş, V. Ahsen, T. Nyokong, *Journal of Photochemistry and Photobiology A: Chemistry* **2007**, 186, 323-329; b) A. Ogunsipe, J.-Y. Chen, T. Nyokong, *New Journal of Chemistry* **2004**, 28, 822-827.
- [15] R. Corporation, Tokyo 196-8666, Japan., **2000-2010**.
- [16] G.M., A64, 112-122. ed., Acta Cryst. , **2008**.